JASA ARTICLE

Spherical oscillations of encapsulated microbubbles: Effect of shell compressibility and anisotropy

Georges Chabouh, Benjamin Dollet, Catherine Quilliet, and Gwennou Coupier[a)]
Université Grenoble Alpes, CNRS, LIPhy, F-38000 Grenoble, France

ABSTRACT:
We introduce a model that describes spherical oscillations of encapsulated microbubbles in an unbounded surrounding fluid. A Rayleigh–Plesset-like equation is derived by coupling the Navier–Stokes equation that describes fluid dynamics with the Navier equation that describes solid dynamics via the internal/external boundary conditions. While previous models were restricted to incompressible isotropic shells, the solid shell is modeled here as a compressible viscoelastic isotropic material and then generalized to an anisotropic material. The exact value of the resonance frequency is calculated analytically, and the damping constant is computed in the approximation of weak damping. A correction of the widely used Church model for incompressible shells is evidenced, and the effects of shell compressibility and anisotropy are discussed. © *2021 Acoustical Society of America*.
https://doi.org/10.1121/10.0003500

(Received 30 June 2020; revised 12 January 2021; accepted 21 January 2021; published online 19 February 2021)

[Editor: Juan Tu] Pages: 1240–1257

I. INTRODUCTION

Various modalities have been used for diagnostic imaging, such as clinical radiography, computed tomography (CT), magnetic resonance imaging (MRI), and ultrasound (US). Safe, noninvasive, and relatively inexpensive, US imaging techniques have been much improved by the introduction of ultrasound micron size contrast agents (UCAs). Image enhancers were essential because, first, human blood within an organ has poor scattering properties and low signal amplitude relative to human tissues, which generate strong echoes, and, second, the old-school Doppler technique (Campbell *et al.*, 1983) could no longer satisfy the demands, especially in some more complex and confined geometries.

The presence of air bubbles inside an injected hand-agitated saline solution during an echocardiography was the first ultrasonic image enhancement technique that was proposed (Gramiak and Shah, 1968). These bubbles are known as the first generation of UCAs. As they dissolve rapidly in the liquid, a second generation of UCAs was developed that are made of air bubbles encapsulated by a thin shell: galactose as in Echovist® (1991) or albumin (a human protein) as in Albunex® (1995) or galactose and palmitic acid as in Levovist® (1995). Finally, the third generation of UCAs includes microbubbles with a longer lifetime, air being simply replaced by a gas with higher molecular weight, responsible for decreased solubility: SF_6 as in SonoVue® (2001), C_3F_8 as in Definity® (2001), or C_4F_{10} as in Sonazoid® (2007). All of these gases are encapsulated by phospholipids. The resulting shells are known as soft-shell UCAs, while the ones made with polymers are known as hard-shell UCAs.

UCAs react to high amplitude pulses (1 MPa) of short duration (on the order of μs). Even in the presence of such agents, axial and lateral resolutions of ultrasonic devices used in clinical applications are limited by diffraction, such that the resolution is fixed by the typical wavelength, which lies between 100 μm and 1 mm in practice. This limit has been strikingly overcome recently: by analyzing the transient signal re-emitted by UCAs, *in vivo* resolution has been decreased to about 10 μm, at a detection frequency high enough to also allow velocity measurement in blood flow by image correlation (Errico *et al.*, 2015). Such a super-resolved technique can also be implemented through a photoacoustic device, where the UCAs are excited by light rather than by sound (Vilov *et al.*, 2017). The scattered US signal of UCAs has also been recently used to discriminate between two network topologies, with application to cancerous tumor detection (Mohanty *et al.*, 2019).

These recent advances are based on a complex interplay between hardware development and post-processing to extract the relevant information from the acquired signal. The response of a shelled bubble is strongly dependent on its size and on the shell material properties. While commercial UCAs are quite polydisperse in size, narrowing the size distribution of UCAs appears then as a way to better match the relatively narrow frequency bandwidth of ultrasonic devices with that of the UCAs, thus leading to better sensitivity of the whole detection process. Recent works go in that direction, making use of shell material of various types, such as polymers (Liu *et al.*, 2014; Song *et al.*, 2018), phospholipids (Gong *et al.*, 2014; Helfield *et al.*, 2014; Lum *et al.*, 2016; Parrales *et al.*, 2014; Segers *et al.*, 2016, 2020; van Rooij *et al.*, 2015) [sometimes forming more than two

[a)]Electronic mail: gwennou.coupier@univ-grenoble-alpes.fr

https://doi.org/10.1121/10.0003500

layers (Shafi *et al.*, 2019)], silica (Hu *et al.*, 2011), or proteins (Wang *et al.*, 2020). This calls for models of bubble oscillations that are able to describe a wide variety of shell materials. While previous ones are focused on incompressible and isotropic material, we present here a model that includes compressibility and the possibility for spherical UCAs to present different material properties in the radial and orthoradial directions ("transverse isotropic" material), a feature that would naturally occur for layered shells like lipidic ones.

Such anisotropy has been shown to greatly influence the buckling process of shells (Munglani *et al.*, 2019; Pitois *et al.*, 2015; Quemeneur *et al.*, 2012).

II. PREVIOUS MODELS

Since the early work of Besant (1859), who was concerned by the time needed to fill up the empty space of a collapsed bubble and the pressure generated at any point in an incompressible liquid, forced vibrations of bubbles have attracted attention for decades. Giving a simpler derivation of Besant's results, Lord Rayleigh (1917) generalized the case to a cavity with nonzero pressure, i.e., to a gas-filled bubble. The surface tension and the viscosity of the surrounding fluid were taken into account [see Plesset and Prosperetti (1977) for a review], leading to the famous Rayleigh–Plesset equation.

To take into account the shell encapsulating the microbubble, a semi-empirical model was developed (de Jong *et al.*, 1994; de Jong *et al.*, 1992) by way of the introduction of two *ad hoc* quantities, S_p and S_f, that account for the effective elastic and dissipative properties of the interface. Assuming a zero-thickness shell, which is motivated by the proximity between the shell thickness and the molecular scale, other models have introduced rheological constants that are explicitly related to the expected properties of the shell material. The first approach by Chatterjee and Sarkar (2003) was followed by the models of Sarkar *et al.* (2005) and Marmottant *et al.* (2005). In the latter, a nonlinear model is proposed, presenting the elasticity of the shell as an effective surface tension. Its linearized form is equivalent to the de Jong model.

In Church (1995), a finite thickness shell was considered. It was assumed to be made of a homogeneous, incompressible, and isotropic material that was described by a Kelvin–Voigt model. This model was linearized relatively to the thickness to radius ratio in Hoff *et al.* (2000), giving rise to the Church–Hoff model. In Morgan *et al.* (2000), thin shell UCAs were described by a constant thickness model using bulk elasticity and viscosity.

Following Marmottant *et al.* (2005), other nonlinear models have been proposed, with a more complex rheological behavior like strain softening and strain hardening (Paul *et al.*, 2010; Tsiglifis and Pelekasis, 2008) or shear thinning (Doinikov *et al.*, 2009; Li *et al.*, 2013).

III. CONFRONTATION WITH EXPERIMENTS

Vibration experiments on UCAs should *a priori* allow the determination of the rheological constants of the material, through the chosen model among those cited above, as long as they are not too numerous. The final goal is usually to choose the best fitting couple of one elastic and one viscous parameter to describe the observed damped signal. This couple is unique for the model selected, for instance, (S_p, S_f) in the de Jong *et al.* (1992) model, (G_S, μ_S) in the Church (1995) model, and so on. Note that using finite thickness shell models requires making assumptions, or additional measurements, to determine the value of the shell thickness. In all models, additional assumptions are generally made in order not to consider the inner gas pressure as an unknown to be determined.

Several techniques can be used to determine the shell oscillations. In Gorce *et al.* (2000), a batch of encapsulated microbubbles are insonated at frequencies up to 30 MHz, and the viscoelastic parameters are deduced by measuring the attenuation expression. The spectroscopy approach relies on using a high speed camera to directly measure the radial displacement of the UCAs, which is fitted with the theoretical one (van der Meer *et al.*, 2007). Light scattering methods were also developed (Li *et al.*, 2013; Tu *et al.*, 2009), where the scattering cross section is related to the resonance frequency containing the viscoelastic properties using the Mie scattering theory. A photoacoustic measurement technique was developed in Lum *et al.* (2016). Readers can refer to Helfield (2019) and Versluis *et al.* (2020) for recent reviews on linear model theory and experimental measuring methods.

All the existing linear models are virtually the same, with 2D moduli that can be expressed explicitly in terms of 3D moduli and thickness. Tables I–IV summarize some experimental estimations of shell properties using the de Jong, Marmottant, Church–Hoff, and Sarkar models, respectively, for different UCAs and using various techniques.

TABLE I. Shell property estimations using de Jong model (de Jong *et al.*, 1992). f and p are the characteristic frequencies and amplitudes of the acoustic waves used to excite the UCAs. S_p and S_f are the elastic and viscous *ad hoc* parameters that are introduced in the model. The intervals for the viscoelastic parameters correspond to cases where dependence on the radius was reported.

UCA	R_{20} (μm)	f (MHz)	p (kPa)	S_p (N/m)	S_f (10^{-6} N/m · s)	Method	Reference
SonoVue®	0.6–4.5	1–10	<10	0.35–2.61	0.46–3.42	Attenuation	Gorce *et al.* (2000)
Albunex®	2.5–6	0.7–12.5	Not known	8	4	Attenuation	de Jong and Hoff (1993)
Definity®	0.5–2.5	12–28	25	1.71	0.015	Attenuation	Goertz *et al.* (2007)
	1–3	7–15	25	1.64	0.15	Attenuation	Faez *et al.* (2011)

TABLE II. Shell property estimations using the Marmottant model (Marmottant *et al.*, 2005). f and p are the characteristic frequencies and amplitudes of the acoustic waves used to excite the UCAs. Analysis of experiments through the model allows determination of the 2D compression modulus χ_{2D} and the surface dilatational viscosity κ_S. In the linearized version of the model, they are related to the constants introduced by de Jong through $S_p = 2\chi_{2D}$ and $S_f = 12\pi\kappa_S$. The intervals for the viscoelastic parameters correspond to cases where dependence on the radius was reported.

UCA	R_{20} (μm)	f (MHz)	p (kPa)	χ_{2D} (N/m)	κ_S (10^{-8} N/m · s)	Method	Reference
SonoVue®	0.975	2.9	130	1	1.5	Spectroscopy	Marmottant *et al.* (2005)
	0.8–3.25	2.5	150	0.024–0.87[a]	0.1–3	Light scattering	Tu *et al.* (2009)
	0.75–3.25	2.5	150	0.39–0.55	0.05–2	Light scattering	Tu *et al.* (2011)
	0.8–3.25	2.5	150	0.4–0.55	0.1–3	Light scattering	Li *et al.* (2013)
BR14®	1.9	1.5–2.5	<40	0.54[a]	2.3	Spectroscopy	van der Meer *et al.* (2007)
Definity®	0.72–1.4	1	308	0.5–0.97	0.01–0.9	Light scattering	Tu *et al.* (2011)
	1.4–2.8	4–13.5	6–25	0.5–2.5	0.02–0.6	Spectroscopy	Helfield and Goertz (2013)
Home-made lipid shell	2.9–6.3	0.5–4		0.28–0.85	3–6	Attenuation	Parrales *et al.* (2014)

[a]Linearized version of the model.

Such experiments may also be used to validate the model that is used to describe the results. This requires determining by another means the rheological properties of the shell material. Such validations are scarce in the literature and yield only accurate order of magnitude so far. Atomic force microscopy (AFM) is a direct approach used to estimate UCAs' properties. However, depending on the model used to extract elastic constants from the force-displacement curve of an AFM, very different values can be found (Abou-Saleh *et al.*, 2013; Buchner Santos *et al.*, 2012; Lytra *et al.*, 2020; Shafi *et al.*, 2019). This makes the validation of spherical oscillation models a tricky task so far. As an example, in Buchner Santos *et al.* (2012) and Lytra *et al.* (2020), values between 8 and 38 MPa are found for the Young modulus E' of a Definity® UCA probed by an AFM. For an incompressible material, the 2D compression modulus χ_{2D} is $E'd_0$, where d_0 is the shell thickness, estimated to be around 5 nm for such UCAs. This leads to $0.04 < \chi_{2D} < 0.2$ N/m, which is not in agreement with the values around 1 N/m found with the de Jong (Table I) or Marmottant (Table II) model. Note, however, that static values of the shell may differ considerably from dynamic values measured in the MHz range.

In addition, experimental determinations have led to unexpected dependences of the viscoelastic parameters on shell radius, as also shown in Tables I–III. van der Meer *et al.* (2007) observed a dependence of the shell viscosity on the initial bubble radius using the Marmottant model for BR14®. Chetty *et al.* (2008) measured an increase in the shear modulus G' with the radius using the Church–Hoff model for SonoVue®. Tu *et al.* (2009) and Li *et al.* (2013) measured an increase in the elasticity and the viscosity parameters of the shell with the shell radius, using the linearized Marmottant model for SonoVue®. Identical observations were made by Doinikov *et al.* (2009) (lipid encapsulated bubbles with the de Jong model), Helfield and Goertz (2013) (Definity® with the Marmottant model), and Parrales *et al.* (2014) (home-made monodisperse encapsulated microbubbles with the linearized Marmottant model).

This dependence on radius of the material properties was not substantiated by physical arguments, suggesting that extra modeling was required.

So far, the models have not considered the possible compressibility or anisotropy of the material constituting the shell. The purpose of the present article is to include these effects in the model of bubble oscillations and to quantify their influence on the linearized oscillation properties, i.e., the eigenfrequency and the damping coefficient.

IV. MODEL

We consider an encapsulated gas bubble immersed in an incompressible fluid with a density ρ_f and a shear viscosity μ_f. The effect of the liquid compressibility could be further included as described in the work of Prosperetti (1987). The bubble shell is modeled as a viscoelastic solid of initial thickness d_e. Furthermore, it was shown according to thin shell theory that a shell made of a homogeneous material with Poisson ratio ν may sustain a maximum relative loss of volume

$$(\Delta V/V)_b = \sqrt{\frac{3(1-\nu)}{1+\nu}}\frac{d_0}{R_{20}} \tag{1}$$

TABLE III. Shell property estimations using the Church–Hoff model (Hoff *et al.*, 2000). The thickness d_0 is an estimation that is made in each paper. f and p are the characteristic frequencies and amplitudes of the acoustic waves used to excite the UCAs. The intervals for the viscoelastic parameters correspond to cases where dependence on the radius was reported.

UCA	R_{20} (μm)	d_0 (nm)	f (MHz)	p (kPa)	G' (MPa)	μ_G (Pa · s)	Method	Reference
SonoVue®	1.78	4	2.5	150	20	0.6	Light scattering	Tu *et al.* (2009)
	3–5.5	2.5	6.8–7.3	40	1.9–105	1	Microscopy	Chetty *et al.* (2008)
Sonazoid®	1.6	4	2–6	300–800	52	0.99	Attenuation	Sarkar *et al.* (2005)
Optison®	1.5	5–10	3.6–4.3	100	20.7	1.7	Attenuation	Chatterjee and Sarkar (2003)

https://doi.org/10.1121/10.0003500

TABLE IV. Shell property estimations using the Sarkar model (Sarkar *et al.*, 2005). f and p are the characteristic frequencies and amplitudes of the acoustic waves used to excite the UCAs. E_S and κ_S are the surface dilatational elasticity and viscosity, respectively, introduced in the model.

UCA	R_{20} (μm)	f (MHz)	p (kPa)	E_S (N/m)	κ_S (10^{-8} N/m · s)	Method	Reference
Sonazoid®	3.2	2–6	200–600	0.51	1	Attenuation	Sarkar *et al.* (2005)
Home-made PLA shell	0.7–1.5	2.5–3	100–150	0.02	0.85	Attenuation	Paul *et al.* (2013)

before it buckles (Hutchinson, 1967; Quilliet, 2012), where d_0 and R_{20} are the shell thickness and external radius at rest, respectively. The first fraction is on the order of 1, except for exotic values of ν close to –1. Even for shells happening to be thicker than the commercially available ones, $(\Delta V/V)_b$ is hence reasonably expected not to exceed 1/10. This point, plus recent experimental results suggesting that pressure-volume relationships obtained within the framework of thin shell theory apply also for thick shells (Coupier *et al.*, 2019), indicates that we may safely consider, here and in the following, that the linear elasticity framework is sufficient to describe the spherical behavior of a wide range of UCAs in the unbuckled regime.

A. Quasi-static approximation

In the absence of body forces, the equation of motion in the solid (Landau and Lifschitz, 1986) reads

$$\rho_S \frac{\partial^2 \boldsymbol{u}}{\partial t^2} - \boldsymbol{\nabla} \cdot \boldsymbol{\sigma} = 0, \tag{2}$$

where ρ_S is the initial density of the solid, $\boldsymbol{u}$ is the displacement field, and $\boldsymbol{\sigma}$ is the Cauchy stress tensor calculated on the actual configuration.

If we consider only elastic contributions to the stress, the dimensional analysis of Eq. (2) shows that if the parameter $\varepsilon = \omega_0^2 d_e^2 \rho_s / E$, which compares the orders of magnitude of the first and second term in Eq. (2), is small, then acceleration can be neglected [see, e.g., Langtangen and Pedersen (2016)]. Here, E is a typical elastic constant of the material, and ω_0 is the (unknown) shell pulsation. Physically, $\sqrt{\varepsilon}$ is the ratio of the typical time scale $\tau_0 = d_e\sqrt{\rho_s/E}$ needed for an elastic wave to travel across the shell thickness d_e over the time scale ω_0^{-1} of the motion of the boundary. In general, E is not smaller than 100 MPa for a polymeric material where $d_e \sim 100$ nm, but for lipid shells of thickness on the order of 5 nm, which are made of the type of anisotropic material that we discuss later in this paper, orders of magnitude as low as 100 kPa were proposed for an effective isotropic Young modulus (Shafi *et al.*, 2019). Hence, with $\rho_S \sim 1000\,\mathrm{kg/m^3}$, τ_0 is expected to be smaller than 5×10^{-10} s. This implies that, with ω_0 usually measured or found according to previous models lower than 10 MHz, ε is lower than 10^{-4}.

The acceleration term can therefore be neglected for actual UCAs and will be so in the rest of this paper. The resolution of Eq. (2) under this assumption will serve to determine the boundary conditions for the stress in the fluid, to determine its acceleration.

A problem similar to ours has been widely studied recently, that of a bubble oscillating in a liquid confined by a viscoelastic solid (Doinikov *et al.*, 2018; Doinikov and Marmottant, 2018; Vincent and Marmottant, 2017; Wang, 2017). A simplifying hypothesis that is used in Vincent and Marmottant (2017) and Wang (2017) is to consider that the surrounding solid is not accelerated by the pressure waves. Here, we have shown that this hypothesis holds for our problem, due in particular to the thinness of the shells.

Note that the resonance frequency ω_0 is the unknown of this problem, so the validity of the hypothesis has to be checked *a posteriori*.

B. Stress-strain relation in the solid

We consider the shell as being made of a transverse isotropic material, i.e., whose properties in the orthoradial plane do not depend on the direction considered but can be different from that in the radial direction. The elastic properties of such a material are characterized by five independent elastic constants. The stress-strain relationship can be written as follows (Lubarda and Chen, 2008):

$$\begin{aligned}\sigma_{ij}^{el} = {} & \lambda\,\epsilon_{kk}\delta_{ij} + 2\mu\,\epsilon_{ij} + 2(\mu_0 - \mu)\,(\delta_{i_0 i}\epsilon_{i_0 j} + \delta_{i_0 j}\epsilon_{i_0 i}) \\ & + \alpha\,(\epsilon_{i_0 i_0}\delta_{ij} + \delta_{i_0 i}\delta_{i_0 j}\epsilon_{kk}) + \beta\,\delta_{i_0 i}\delta_{i_0 j}\epsilon_{i_0 i_0},\end{aligned} \tag{3}$$

where ϵ is the strain tensor, λ is the first Lamé coefficient, μ is the shear modulus in the plane of isotropy, μ_0 is the out-of-plane shear modulus, and α and β are two other coefficients. The direction i_0 points the axis of transverse isotropy. For an isotropic material, $\alpha = \beta = 0$ and $\mu_0 = \mu$. For radial displacements, the elastic Cauchy stress tensor has only diagonal components given by

$$\begin{cases} \sigma_{rr}^{el} = (\lambda + 4\mu_0 - 2\mu + 2\alpha + \beta)\,\epsilon_{rr} + 2(\lambda + \alpha)\,\epsilon_{\theta\theta}, \\ \sigma_{\theta\theta}^{el} = \sigma_{\phi\phi}^{el} = (\lambda + \alpha)\,\epsilon_{rr} + 2(\lambda + \mu)\,\epsilon_{\theta\theta}, \end{cases} \tag{4}$$

with $\epsilon_{rr} = \partial u/\partial r$ and $\epsilon_{\theta\theta} = \epsilon_{\phi\phi} = u/r$, where $u = u(r,t)$ is the Eulerian radial displacement in the shell.

The viscoelastic properties of the material are described by the generalized Kelvin–Voigt model (Thompson and Kelvin, 1865; Voigt, 1892), where the complete strain tensor reads $\boldsymbol{\sigma} = \boldsymbol{\sigma}^{el} + \boldsymbol{\sigma}^{visc}$, where $\boldsymbol{\sigma}^{visc}$ is the viscous stress. For a transverse anisotropic material, integrating a thermodynamically consistent model (Dalenbring, 2002) based on the augmented Hooke's law (AHL) (Dovstam, 1995) in this fluid-structure interaction problem requires finite element implementation. Another approach may be to consider

viscosity effect for only some components of the stress tensor (Lubarda and Asaro, 2014).

We will therefore consider two cases in this paper, both going one step further compared to the model by Church (1995) that considers an isotropic and incompressible material:

(1) A viscoelastic isotropic material, which can be compressible,
(2) An anisotropic, purely elastic, material, which is transversely isotropic and compressible.

In the case of an isotropic linear material, the elastic stress reads

$$\begin{cases} \sigma_{rr}^{el} = \left(K' + \frac{4}{3}G'\right)\epsilon_{rr} + 2\left(K' - \frac{2}{3}G'\right)\epsilon_{\theta\theta}, \\ \sigma_{\theta\theta}^{el} = \sigma_{\phi\phi}^{el} = \left(K' - \frac{2}{3}G'\right)\epsilon_{rr} + 2\left(K' + \frac{1}{3}G'\right)\epsilon_{\theta\theta}, \end{cases} \tag{5}$$

where we have introduced the shear modulus $G' = \mu$ and the bulk modulus $K' = \lambda + \frac{2}{3}\mu$. Both are *a priori* functions of the oscillation frequency, which would call for the resolution of a self-consistency equation when the oscillation frequency will be eventually found as a function of, in particular, these elastic constants. We introduce the Kelvin–Voigt viscous stress $\boldsymbol{\sigma}^{visc}$ whose expression is similar to that of the elastic stress:

$$\begin{cases} \sigma_{rr}^{visc} = \left(\mu_K + \frac{4}{3}\mu_G\right)\dot{\epsilon}_{rr} + 2\left(\mu_K - \frac{2}{3}\mu_G\right)\dot{\epsilon}_{\theta\theta}, \\ \sigma_{\theta\theta}^{visc} = \sigma_{\phi\phi}^{visc} = \left(\mu_K - \frac{2}{3}\mu_G\right)\dot{\epsilon}_{rr} + 2\left(\mu_K + \frac{1}{3}\mu_G\right)\dot{\epsilon}_{\theta\theta}. \end{cases} \tag{6}$$

The viscosities μ_K and μ_G describe the friction losses due to volume changes and shear, respectively. Little is known, in general, about the values of the loss moduli and, in particular, the "viscous Poisson ratio," whose definition may vary depending on the authors (Lakes and Wineman, 2006). Its determination generally requires the performance of two independent experiments aiming at determining, e.g., a shear loss modulus G'' and a traction loss modulus E'' [see, e.g., Guillot and Trivett (2011)]. From a modeling perspective, one approach consists in following Lemaitre and Chaboche (1994), where it is assumed, with no explicit justification, that the ratio μ_K/μ_G is equal to K'/G', which amounts to saying that the viscous Poisson ratio that would characterize a ratio of strain rates is equal to the elastic Poisson ratio that characterizes the ratio of strains (Linn *et al.*, 2013; von Ende *et al.*, 2011). Without this assumption, and considering an AHL model as in Tschoegl *et al.* (2002), Pritz (2009) has proposed bounds for the potential values of the loss moduli for materials with a positive Poisson ratio and a low enough shear loss factor. He shows that $2/3 < K''/G'' < 1$, which, for a sinusoidal signal of given pulsation w_0, amounts to the tight inequalities $2/3 < \mu_K/\mu_G < 1$. We discuss these two assumptions in Sec. V J, but one should keep in mind that the difficulties in characterizing accurately two dissipation constants in viscoelastic materials, whose properties are often frequency dependent, must lead to consideration of the aforementioned relationships as pure hypotheses for now.

V. ISOTROPIC COMPRESSIBLE SHELL

A. Deformation in the solid

The Eulerian radial displacement u within the shell is defined on the actual configuration as the variation from an unstrained position holding no stress within the shell,

$$u(r,t) = r - r_e, \tag{7}$$

where r is the actual position of a material particle located at r_e in the reference configuration.

The radial displacement $u(r, t)$ is then calculated by solving Eq. (2) in the quasi-static approximation:

$$\left[\boldsymbol{\nabla}\cdot\left(\boldsymbol{\sigma}^{el} + \boldsymbol{\sigma}^{visc}\right)\right]_r = 0. \tag{8}$$

The ratio between the viscous and the elastic terms in the above equation is given by the ratio between the loss and storage moduli. Previous experimental studies on existing UCAs show that the ratio between the viscosity and the storage modulus is on the order of $10^{-8} - 10^{-9}$ s (see values in Tables I–IV); therefore, $\omega_0\tau_S$ is often small, which we will take as a hypothesis in the following.

For an isotropic solid, from $[\boldsymbol{\nabla}\cdot\boldsymbol{\sigma}]_r = (\partial\sigma_{rr}/\partial r) + (2/r)(\sigma_{rr} - \sigma_{\theta\theta})$ and using Eqs. (5) and (6), we are led to solve

$$\left(\frac{\partial^2}{\partial r^2} + \frac{2}{r}\frac{\partial}{\partial r} - \frac{2}{r^2}\right)(u + \tau_S\dot{u}) = 0, \tag{9}$$

with

$$\tau_S = \frac{\mu_M}{M'},\ M' = K' + \frac{4}{3}G',\ \mu_M = \mu_K + \frac{4}{3}\mu_G. \tag{10}$$

The solutions of Eq. (9) can be written as

$$u(r,t) = a(t)r + \frac{b(t)}{r^2} + A(r)e^{-t/\tau_S}, \tag{11}$$

where the term in $A(r)$ characterizes the internal relaxation within the shell. Note that since $\omega_0\tau_S$ is small, this term will marginally contribute to the overall response of the shell, and we shall therefore place ourselves in the conditions where it is zero.

The two variables $a(t)$ and $b(t)$ depend on the long time $t \gg \tau_S$ associated with the variations of the boundary conditions. We first express them as functions of $R_1(t)$ and $R_2(t)$, respectively the internal and external radii of the shell, which are our variables of interest. This is achieved thanks

https://doi.org/10.1121/10.0003500

to Eq. (7), which leads to $u(R_i) = R_i(t) - R_{ie}$, for $i = 1, 2$. R_{1e} and R_{2e} are the values of the radii in the unstrained case, and R_{10} and R_{20} are their values at equilibrium in the fluid, which may differ from R_{1e} and R_{2e}, notably because of hydrostatic pressure. We find

$$a(t) = \frac{R_2^2(t)[R_2(t) - R_{2e}] - R_1^2(t)[R_1(t) - R_{1e}]}{R_2^3(t) - R_1^3(t)}, \tag{12}$$

and

$$b(t) = \frac{R_1^2(t)R_2^2(t)}{R_2^3(t) - R_1^3(t)}\{R_2(t)[R_1(t) - R_{1e}] - R_1(t)[R_2(t) - R_{2e}]\}. \tag{13}$$

Note that a and b are on the order of 1 relative to the displacements at the boundaries, in agreement with the linear elastic theory used here to characterize the deformation tensor.

B. Velocity in the solid

The velocity field in the shell $\boldsymbol{v}_s$ is the material derivative of the Eulerian displacement $\boldsymbol{u}(r, t)$:

$$\boldsymbol{v}_s(r, t) = \frac{D\boldsymbol{u}}{Dt} = \frac{\partial \boldsymbol{u}}{\partial t} + \boldsymbol{\nabla u} \cdot \boldsymbol{v}_s(r, t). \tag{14}$$

For small deformations, $|\boldsymbol{\nabla u}| \ll 1$, the radial component of the velocity v_s thus can be approximated to

$$v_s \approx \frac{\partial u}{\partial t} = \dot{a}r + \frac{\dot{b}}{r^2}, \tag{15}$$

where $\dot{a}$ and $\dot{b}$ are the time derivative of the variables a and b. Direct calculation of $\dot{a}$ and $\dot{b}$, shown in the Appendix, leads to expressions that violate the kinematic boundary conditions, i.e., $v_s(r = R_1) \neq U_1$ and $v_s(r = R_2) \neq U_2$, where we define $U_1 = \dot{R}_1$ and $U_2 = \dot{R}_2$. However, the deviations from the kinematic boundary conditions remain on the order of $|R_i - R_{ie}|/R_{ie}$, consistent with the assumption of small deformation and linear elastic behavior. Hence, we can restrict the velocity to its leading order expression, where R_{1e} coincides with R_1 and R_{2e} with R_2. This leads to an expression for v_s that can otherwise be obtained directly from Eq. (15) by applying continuity condition at R_1 and R_2:

$$v_s(r, t) \approx a_v r + \frac{b_v}{r^2}, \tag{16}$$

where

$$a_v = \frac{R_2^2(t)U_2 - R_1^2(t)U_1}{R_2^3(t) - R_1^3(t)}, \tag{17}$$

and

$$b_v = \frac{[R_2(t)U_1 - R_1(t)U_2]R_1^2(t)R_2^2(t)}{R_2^3(t) - R_1^3(t)}. \tag{18}$$

The above calculated displacement and velocity generalize the ones found in Church (1995), where an incompressible solid material is considered. Such materials are characterized by a traceless deformation tensor,

$$\epsilon_{rr} + \epsilon_{\theta\theta} + \epsilon_{\phi\phi} = 3a = 0, \tag{19}$$

leading to the following displacement in the solid:

$$u^{\text{inc}}(r, t) = \frac{R_1^2(t)[R_1(t) - R_{1e}]}{r^2}, \tag{20}$$

where we have also used the relation $a = 0$ to reformulate the expression of b. The velocity v_s given by Eq. (16) then becomes

$$v_s^{\text{inc}}(r, t) = \frac{R_1^2(t)U_1}{r^2}. \tag{21}$$

Equations (20) and (21) are identical to the ones found in Church (1995), where the solid velocity was calculated directly from the law of conservation of the mass for an incompressible fluid, $\boldsymbol{\nabla} \cdot \boldsymbol{v}_s = 0$, while the displacement was deduced from volume conservation that reads, in the small deformation limit, $\boldsymbol{\nabla} \cdot \boldsymbol{u} = 0$. Note that the two approaches are cross-consistent only in the small deformation framework: then in this case, $\boldsymbol{\nabla} \cdot \boldsymbol{u} = 0$, and moreover the $1/r^2$ behavior of v_s is recovered only if Eq. (14) is approximated to Eq. (15).

Note finally that the displacement can also be defined on the reference configuration, i.e., using Lagrangian formalism without significant difference (Altenbach *et al.*, 2008).

C. Equations of motion in the liquid

The conservation of mass for an incompressible fluid in a spherical coordinate system gives

$$\frac{1}{r^2}\frac{\partial}{\partial r}(r^2 \mathbf{v}) = 0, \tag{22}$$

where $\mathbf{v} = (v_f(r), 0, 0)$ is the radial Eulerian velocity vector in the fluid. For $r = R_2$, $v_f(r = R_2) \equiv U_2$.

The velocity profile of the fluid is then

$$v_f(r) = \frac{U_2 R_2^2}{r^2}. \tag{23}$$

The Navier–Stokes equation for an incompressible fluid and irrotational flow reads (Landau and Lifschitz, 1987)

$$\rho_f\left(\frac{\partial v_f}{\partial t} + v_f\frac{\partial v_f}{\partial r}\right) = -\frac{\partial P}{\partial r}. \tag{24}$$

Integration of Eq. (24) between R_2 and $+\infty$, using Eq. (23), leads to

$$\rho_f\left(R_2\dot{U}_2 + \frac{3}{2}U_2^2\right) = P_{f|_{r=R_2}} - P_\infty, \tag{25}$$

where $P_{f|_{r=R_2}}$ is the pressure in the fluid near the shell boundary, and P_∞ is the sum of the applied acoustic pressure $P_{ac}(t)$ and the ambient pressure P_0.

In addition, conservation of radial momentum at the external surfaces of the shell imposes

$$-P_G(t) = (\sigma_{rr}^{el} + \sigma_{rr}^{visc})|_{r=R_1} - \frac{2\gamma_1}{R_1} \tag{26}$$

and

$$(\sigma_{rr}^{el} + \sigma_{rr}^{visc})|_{r=R_2} = -P_f|_{r=R_2} + \sigma_{rr}^{f}|_{r=R_2} - \frac{2\gamma_2}{R_2}, \tag{27}$$

where γ_1 and γ_2 are the surface tensions, respectively at the internal and external boundaries of the shell, and $P_G(t)$ is the pressure of the gas inside the bubble. We assume the gas obeys a polytropic law, such that $P_G(t) = P_{g_0}(R_{10}/R_1)^{3\kappa}$, where P_{G_0} is the equilibrium gas pressure and κ is the polytropic exponent of the gas. The radial component σ_{rr}^f of the viscous stress equals

$$\sigma_{rr}^f = 2\mu_f \frac{\partial v_f}{\partial r} = -4\mu_f \frac{U_2 R_2^2(t)}{r^3}. \tag{28}$$

The normal stresses in the shell are obtained from Eqs. (5), (6), (11), and (15), noting that as done for the velocity, the strain rate $\dot{\epsilon}$ is approximated in the linear elasticity limit to $\dot{\epsilon} = \partial\epsilon/\partial t$; therefore, the relation between $\dot{\epsilon}$ and v_s is similar to that between ϵ and u. We have then

$$\sigma_{rr}^{el} = 3K'a - 4G'\frac{b}{r^3}, \tag{29}$$

$$\sigma_{rr}^{visc} = 3\mu_K a_v - 4\mu_G \frac{b_v}{r^3}. \tag{30}$$

Inserting Eqs. (29) and (30) in the first boundary condition (26) leads to a first equation for R_1 and R_2:

$$-P_G + 2\frac{\gamma_1}{R_1} = 3K'a - 4G'\frac{b}{R_1^3} + 3\mu_K a_v - 4\mu_G \frac{b_v}{R_1^3}. \tag{31}$$

Replacing a, b, a_v, and b_v with their values (12, 13, 17, and 18) in the above equation, one eventually gets

$$\begin{aligned} -P_G + 2\frac{\gamma_1}{R_1} = {} & 3K'\frac{R_2^2(R_2 - R_{2e}) - R_1^2(R_1 - R_{1e})}{R_2^3 - R_1^3} \\ & -4G'\frac{[R_2(R_1 - R_{1e}) - R_1(R_2 - R_{2e})]R_2^2}{(R_2^3 - R_1^3)R_1} \\ & +3\mu_K \frac{R_2^2 U_2 - R_1^2 U_1}{R_2^3 - R_1^3} \\ & -4\mu_G \frac{(R_2 U_1 - R_1 U_2)R_2^2}{(R_2^3 - R_1^3)R_1}. \end{aligned} \tag{32}$$

We use the second boundary condition (27) to get rid of the unknown fluid pressure in Eq. (25), such that

$$\begin{aligned} \rho_f\left(R_2\dot{U}_2 + \frac{3}{2}U_2^2\right) = {} & -\frac{2\gamma_2}{R_2} - P_\infty - 4\mu_f\frac{U_2}{R_2} \\ & -3K'a + 4G'\frac{b}{R_2^3} - 3\mu_K a_v + 4\mu_G\frac{b_v}{R_2^3}. \end{aligned} \tag{33}$$

This equation can be rewritten in a form that resembles a Rayleigh–Plesset equation by replacing the term $R_2 - R_{2e}$ in a and b thanks to Eq. (32):

$$\begin{aligned} & \rho_f\left(R_2\dot{U}_2 + \frac{3}{2}U_2^2\right) \\ & = -P_0 - P_{ac}(t) - 2\frac{\gamma_2}{R_2} - 4\mu_f\frac{U_2}{R_2} \\ & \quad + \left(P_G - 2\frac{\gamma_1}{R_1}\right)\left(1 - \frac{4G'}{3K' + 4G'}\frac{R_2^3 - R_1^3}{R_2^3}\right) \\ & \quad -4G'\frac{3K'}{3K' + 4G'}\frac{R_2^3 - R_1^3}{R_2^3}\frac{R_1 - R_{1e}}{R_1} \\ & \quad +4\frac{U_2}{R_2}\left[\mu_G\left(1 - \frac{4G'}{3K' + 4G'}\right) - \mu_K\frac{3G'}{3K' + 4G'}\right] \\ & \quad -4\frac{U_1}{R_1}\left[\mu_G\left(1 - \frac{4G'}{3K' + 4G'}\right) - \mu_K\frac{3G'}{3K' + 4G'}\frac{R_1^3}{R_2^3}\right]. \end{aligned} \tag{34}$$

In this expression, it is interesting to observe that the elastic contribution of the internal gas is modulated by the intrinsic elastic properties of the shell. This feature will disappear in the incompressible limit. Equations (32) and (34) constitute a system of differential equations for the two unknowns R_1 and R_2. For incompressible materials, the Rayleigh–Plesset equation is sufficient, as R_1 and R_2 are simply linked through the incompressibility condition.

D. Unstrained *vs* initial radii

As mentioned before, the unstrained radii may be different from the initial radii: $R_{ie} \neq R_{i0}$. The radius R_{ie} is defined by the unstrained state of the shell before it is plunged into the liquid, after what stresses within the shell take place, due to the surface tension at the interfaces, and the internal and external pressures.

Taking Eqs. (32) and (34) at equilibrium ($U_1 = U_2 = 0$, $P_\infty = P_0$), one can extract the displacements $R_{i0} - R_{ie}$. They can be written $R_{1e} = R_{10}(1 + Z_1)$ and $R_{2e} = R_{20}(1 + Z_2)$, with

$$\begin{aligned} Z_1 = {} & \frac{1}{3K'}\left[\frac{R_{20}^3}{\hat{V}_S}\left(P_0 + \frac{2\gamma_2}{R_{20}}\right) - \frac{R_{10}^3}{\hat{V}_S}\left(P_{G_0} - \frac{2\gamma_1}{R_{10}}\right)\right] \\ & \times \frac{1}{4G'}\left[\frac{R_{20}^3}{\hat{V}_S}\left(P_0 - P_{G_0} + \frac{2\gamma_2}{R_{20}} + \frac{2\gamma_1}{R_{10}}\right)\right], \end{aligned} \tag{35}$$

https://doi.org/10.1121/10.0003500

$$Z_2 = \frac{1}{3K'}\left[\frac{R_{20}^3}{\hat{V}_S}\left(P_0 + \frac{2\gamma_2}{R_{20}}\right) - \frac{R_{10}^3}{\hat{V}_S}\left(P_{G_0} - \frac{2\gamma_1}{R_{10}}\right)\right] \times \frac{1}{4G'}\left[\frac{R_{10}^3}{\hat{V}_S}\left(P_0 - P_{G_0} + \frac{2\gamma_2}{R_{20}} + \frac{2\gamma_1}{R_{10}}\right)\right], \quad (36)$$

where $\hat{V}_S = R_{20}^3 - R_{10}^3$.

These formulations highlight the effect of compressibility, which is the same for the two radii.

If the shell is incompressible ($K' \gg P_{G_0}, P_0, \gamma_i/R_{10}$), one has

$$Z_i^{inc} = \left(P_0 - P_{G_0} + \frac{2\gamma_1}{R_{10}} + \frac{2\gamma_2}{R_{20}}\right)\frac{R_{20}^3 + R_{10}^3 - R_{i0}^3}{4G'\hat{V}_S}, \quad (37)$$

which is identical to the expression found in Church (1995) when $P_{G_0} = P_0$, which was hypothesized in that paper.

In Doinikov and Dayton (2006), where incompressible shells are also considered, the authors find the same relation as Eq. (37), which is the first order of their Eq. (33). However, in a second step, they go further in the calculation using deformation profiles that are valid in the compressible case and find expressions [Eqs. (40) and (41) in their paper] that contradict our findings and the ones in Church (1995) and in Sarkar *et al.* (2005) in that they find the counterintuitive result that surface tension tends to increase the equilibrium radius. Here, we are satisfied with the observation that an increase in surface tension leads to a shrinkage of the shell. This altogether suggests that care must be taken not to mix expressions from the compressible case with expressions from the incompressible case.

It is worth emphasizing that in the incompressible case, the ratio of the volume in the unstressed configuration to that after the shell is plunged in the fluid, namely $[R_{20}^3(1+Z_2^{inc})^3 - R_{10}^3(1+Z_1^{inc})^3]/(R_{20}^3 - R_{10}^3)$, is equal to 1 in this model or in the other models (Church, 1995; Doinikov and Dayton, 2006; Khismatullin and Nadim, 2002) only to first order in Z_i^{inc}. This corresponds to the domain of validity of the linear elasticity framework. In the general case, one must therefore restrict the obtained expressions to the first order in Z_i for consistency.

E. Linear analysis

Assuming a small-amplitude oscillation, linear equations for the R_i can be obtained using the following relations:

$$\begin{aligned} &R_1(t) = R_{10}[1 + x(t)],\ |x(t)| \ll 1;\\ &R_2(t) = R_{20}[1 + y(t)],\ |y(t)| \ll 1;\\ &U_1(t) = R_{10}\dot{x};\\ &U_2(t) = R_{20}\dot{y}. \end{aligned} \quad (38)$$

Keeping only the first-order terms in x, y, Z_1, and Z_2, and using Eqs. (35) and (36), Eq. (32) becomes,

$$-\left(3\kappa P_{G_0} - \frac{2\gamma_1}{R_{10}} + \frac{4G'R_{20}^3 + 3K'R_{10}^3}{R_{20}^3 - R_{10}^3}\right)x + \frac{(4G' + 3K')R_{20}^3}{R_{20}^3 - R_{10}^3}y - \frac{4\mu_G R_{20}^3 + 3\mu_K R_{10}^3}{R_{20}^3 - R_{10}^3}\dot{x} + \frac{(4\mu_G + 3\mu_K)R_{20}^3}{R_{20}^3 - R_{10}^3}\dot{y} = 0. \quad (39)$$

Dividing this equation by K' and taking the limit $K' \to \infty$, one gets $x = yR_{20}^3/R_{10}^3$, which is the relationship obtained for an incompressible material as in Church (1995). Equation (39) is therefore a generalization of this relationship for the case of a viscoelastic compressible material.

Equation (39) together with the linearized Rayleigh–Plesset-like equation obtained from Eq. (34) constitutes the following linear system:

$$M\ddot{X} + B\dot{X} + KX = F(t), \quad (40)$$

where

$$X = \begin{pmatrix} x \\ y \end{pmatrix},\ F(t) = \begin{pmatrix} -P_{ac}(t) \\ 0 \end{pmatrix},\ M = \begin{bmatrix} 0 & \rho_f R_{20}^2 \\ 0 & 0 \end{bmatrix},$$
$$B = \begin{bmatrix} b_{11} & b_{12} \\ \dfrac{-4\mu_G R_{20}^3 - 3\mu_K R_{10}^3}{R_{20}^3 - R_{10}^3} & \dfrac{(4\mu_G + 3\mu_K)R_{20}^3}{R_{20}^3 - R_{10}^3} \end{bmatrix}$$

with

$$b_{11} = 12\frac{K'\mu_G - G'\mu_K\dfrac{R_{10}^3}{R_{20}^3}}{3K' + 4G'},$$
$$b_{12} = 4\left(\mu_f + 3\frac{K'\mu_G - G'\mu_K}{3K' + 4G'}\right), \quad (41)$$

and

$$K = \begin{bmatrix} k_{11} & \dfrac{-2\gamma_2}{R_{20}} \\ k_{21} & \dfrac{(4G' + 3K')R_{20}^3}{R_{20}^3 - R_{10}^3} \end{bmatrix} \quad (42)$$

with

$$k_{11} = \left(3\kappa P_{G_0} - \frac{2\gamma_1}{R_{10}}\right)\left(1 - \frac{4G'}{3K' + 4G'}\frac{R_{20}^3 - R_{10}^3}{R_{20}^3}\right) + \frac{12G'K'}{3K' + 4G'}\frac{R_{20}^3 - R_{10}^3}{R_{20}^3},$$
$$k_{21} = -3\kappa P_{G_0} + \frac{2\gamma_1}{R_{10}} - \frac{4G'R_{20}^3 + 3K'R_{10}^3}{R_{20}^3 - R_{10}^3}. \quad (43)$$

The free oscillations of the shells ($Pac = 0$) are described by non-trivial harmonic solutions of the above system $X = X_0 e^{\lambda t}$, where $\lambda = -\delta + i\omega$, that are obtained by

setting $\det(\lambda^2 M + \lambda B + K) = 0$. This leads to a polynomial equation on the order of 3 for λ, which can be solved analytically (yet leading to very long expressions) or numerically. This equation reads

$$c_1\lambda^3 + c_2\lambda^2 + c_3\lambda + c_4 = 0, \tag{44}$$

where

$$\begin{aligned} &c_1 = -b_{21}m_{12}, \quad c_2 = \det[B] - k_{21}m_{12}, \\ &c_3 = b_{11}k_{22} - b_{12}k_{21} - b_{21}k_{12} + b_{22}k_{11}, \quad c_4 = \det[K]. \end{aligned} \tag{45}$$

For the sake of comparison with the literature, and making use of the observation that the damping coefficient is usually small, we present the leading order approximation and the first-order correction with respect to this damping coefficient in the following. Note that this is a second and independent approximation, based on the usual values of dissipation factors, that is added to that of small deformation.

F. Leading order approximation

For $B = 0$, Eq. (44) becomes $\det[K] - k_{21}m_{12}\lambda^2 = 0$; therefore, $\lambda = i\omega_0$, where the undamped resonance frequency ω_0 is given by

$$\begin{aligned} \omega_0^2 = \frac{3K' + 4G'}{\rho_f R_{20}^2} &\left[4G' \frac{3K'}{3K' + 4G'} \frac{R_{20}^3 - R_{10}^3}{R_{20}^3} \right. \\ &\left. + \left(3\kappa P_{G0} - \frac{2\gamma_1}{R_{10}}\right)\left(1 - \frac{4G'}{3K' + 4G'} \frac{R_{20}^3 - R_{10}^3}{R_{20}^3}\right) \right] \\ &\times \left[\left(3\kappa P_{G0} - \frac{2\gamma_1}{R_{10}}\right) \frac{R_{20}^3 - R_{10}^3}{R_{20}^3} + 4G' + 3K' \frac{R_{10}^3}{R_{20}^3} \right]^{-1} \\ &- \frac{2\gamma_2}{\rho_f R_{20}^3}. \end{aligned} \tag{46}$$

This constitutes the central result of this paper. The last term in the above expression is the classical contribution of the surface tension of the outer surface, which acts against an effective mass of fluid whose scale is given by the shell size. By contrast, the contribution of the shell elasticity and of the elastic forces acting on the inner side of the shell (the gas pressure and the surface tension) are strongly coupled. As discussed later, this coupling disappears in the incompressibility limit. As in the Rayleigh–Plesset expression for a free bubble—$\omega_0^{RP} = [\frac{1}{\rho_f R_{20}^2}(3\kappa P_{G0} - \frac{2\gamma_1}{R_{20}} - \frac{2\gamma_2}{R_{20}})]^{1/2}$, which is recovered here with Eq. (46) taken in the limit of vanishing shell volume ($R_{10} \to R_{20}$)—adding surface tension makes the shell pulsation decrease, at *fixed* P_{G0}. In practice, P_{G0} is not known or measurable, and it would be preferable to express the pulsation as a function of the external pressure P_0. While this is easily done for a free bubble, leading to an increase in pulsation with surface tensions, this is more complex in the present situation: P_{G0} and P_0 also couple through the elastic stress within the shell, which depends on the reference configuration (R_{1e}, R_{2e}), which is not known in general.

In this context, measuring oscillation frequency cannot be sufficient to determine the elastic constants of the shell material. Even if surface tensions are assumed to be zero, and considering that the external radius is known, we are left with four unknowns, which are the two elastic constants, the internal pressure and the internal radius. This is one more than in the Church model and two more than in zero-thickness shell models. Even in these simpler models, and in all cases, one needs to know more about the fabrication process of the shell to know their stress-free state or to make additional assumptions. In Church (1995), it is for instance assumed that permeability of the shell under study allows us to consider that $P_{G0} = P_0$, which may be true for thin lipid shells, but not for thicker shells, as pointed out in Doinikov and Dayton (2006).

For an incompressible shell, the undamped natural frequency becomes

$$\begin{aligned} \omega_0^{inc} = (\rho_S R_{10}^2 \alpha^{inc})^{-1/2} &\left(3\kappa P_{G0} - \frac{2\gamma_1}{R_{10}} - \frac{2\gamma_2}{R_{20}} \frac{R_{10}^3}{R_{20}^3} \right. \\ &\left. + 4G' \frac{R_{20}^3 - R_{10}^3}{R_{20}^3} \right)^{1/2}, \quad \text{with} \quad \alpha^{inc} = \frac{\rho_f}{\rho_S} \frac{R_{10}}{R_{20}}. \end{aligned} \tag{47}$$

This differs from the expression proposed in Church (1995):

$$\begin{aligned} \omega_0^{Ch} = (\rho_S R_{10}^2 \alpha^{Ch})^{-1/2} &\left\{ 3\kappa P_{G0} - \frac{2\gamma_1}{R_{10}} - \frac{2\gamma_2}{R_{20}} \frac{R_{10}^3}{R_{20}^3} \right. \\ &\left. + 4G' \frac{R_{20}^3 - R_{10}^3}{R_{20}^3} \left[1 + Z_1^{Ch} \left(1 + \frac{3R_{10}^3}{R_{20}^3} \right) \right] \right\}^{1/2}, \end{aligned} \tag{48}$$

with

$$\alpha^{Ch} = \frac{\rho_f}{\rho_S} \frac{R_{10}}{R_{20}} + 1 - \frac{R_{10}}{R_{20}}. \tag{49}$$

The first difference lies in the effective mass characterized by the coefficient α, since we neglected the inertia of the shell. Note that it introduces a correction on ω_0^2 on the order of d_0/R_{20}, where $d_0 = R_{20} - R_{10}$, that is of at most a few percent for actual UCAs.

The other difference lies in the presence of a Z_1^{Ch} term in Church (1995). This is due to a subtle inconsistency in the linearizing process: as discussed in Sec. V D, Z_1^{Ch} must be considered as a small parameter to keep the validity of the linear elasticity framework. It characterizes the difference between the unstrained state and the equilibrium state, the same way as x and y in Eq. (38) characterize the difference between the actual and the equilibrium state. Terms like xZ_1 should therefore not be included in the linearized

https://doi.org/10.1121/10.0003500

equation, contrary to what is done in Church (1995) between his Eqs. (12) and (17). Replacing Z_1^{Ch} by its value in ω_0^{Ch}, one gets

$$\omega_0^{Ch} = (\rho_S R_{10}^2 \alpha^{Ch})^{-1/2} \left[3\kappa P_{G0} + \frac{2\gamma_1}{R_{10}} \frac{3R_{10}^3}{R_{20}^3} + \frac{2\gamma_2}{R_{20}} \left(1 + \frac{2R_{10}^3}{R_{20}^3} \right) + 4G' \left(\frac{R_{20}^3 - R_{10}^3}{R_{20}^3} \right) \right]^{1/2}. \tag{50}$$

One can see that the contributions of the surface tension are incorrectly estimated with this contested expression by Church, as this expression does not converge to the Rayleigh–Plesset pulsation ω_0^{RP} in the vanishing volume limit.

G. First-order approximation

If Eq. (44) is expanded to the first orders in b_{ij} and δ, one gets that $\omega = \omega_0$ and

$$\delta = -\frac{c_3 + b_{21} m_{12} \omega_0^2}{2k_{21} m_{12}}, \tag{51}$$

which can be reformulated as

$$\delta = \frac{1}{2m_{12}} \left[b_{12} - b_{11} \frac{k_{22}}{k_{21}} + \frac{k_{11}}{k_{21}^2} (b_{21} k_{22} - b_{22} k_{21}) \right]. \tag{52}$$

As seen in Eq. (40), the first term b_{12} in the above expression represents the damping directly affecting the motion of the external radius of the shell, through the fluid viscosity and a contribution of the shell viscosity. The second term stems from the damping affecting the motion of the internal radius, which is weighted by the elastic contribution k_{22}/k_{21}. The third term stems from the coupling between dissipation and elastic deformation inside the shell.

For an incompressible shell, the damping ratio δ in Eq. (51) simply becomes

$$\delta^{inc} = 2 \frac{(R_{20}^3 - R_{10}^3)\mu_G + R_{10}^3 \mu_f}{\rho_S R_{10}^2 R_{20}^3 \alpha^{inc}}. \tag{53}$$

In Church (1995), it reads

$$\delta^{Ch} = 2 \frac{(R_{20}^3 - R_{10}^3)\mu_G + R_{10}^3 \mu_f}{\rho_S R_{10}^2 R_{20}^3 \alpha^{Ch}}. \tag{54}$$

As for the pulsation, a difference of a few percent remains, which is related to the absence of shell mass in our model.

H. Discussion: Effect of compressibility on ω_0

We discuss in this section to what extent the frequency is modified when the material is compressible. We first consider a reference configuration, denoted $\mathcal{R}$, which is considered in Church (1995): $d_0 = 15$ nm, $P_{G_0} = 101.3$ kPa, $\rho_f = 1000\,\mathrm{kg/m^3}$, $\rho_S = 1100\,\mathrm{kg/m^3}$, $\mu_f = 0.001$ Pa·s, $G' = 88.8$ MPa, $\gamma_1 = 0.04$ N/m, $\gamma_2 = 0.005$ N/m, and $\kappa = 7/5$. For such a shell whose external radius lies in the range 1–10 μm, we find that $0.99 < \omega_0^{inc}/\omega_0^{Ch} < 1$, which indicates that while our model has led us to neglect the inertia of the shell, this assumption will modify the final result by a negligible amount. Note that in this example, since $\gamma_i/R_{i0} \ll G'$, the inaccuracy that we exhibited in the Church (1995) model has no quantitative consequence. In the following, we consider ω_0^{inc} as the reference value for discussion.

We now discuss the effect of compressibility together with an evaluation of the impact of the contribution of gas compressibility. For most commercial shells, G' is actually 10–1000 times the ambient pressure (see, e.g., Table III). Since the G' contribution is weighted by d / R (which is roughly the ratio of the shell material volume over the volume of gas), both contributions are likely to contribute with comparable weight.

As the contribution of the external surface tension is purely additive, for simplicity we set $\gamma_2 = 0$ and consider several values of $\tilde{P} = P_{G_0} - (2\gamma_1/3\kappa R_{10})$, which characterizes the contribution of the inner gas to UCA oscillations. In this case, regarding space variables, $R_{20} \times \omega_0$ depends only on d_0/R_{20}.

In Fig. 1, the ratio ω_0/ω_0^{inc} is calculated for different values of G' and K', which are set relatively to $\tilde{P}$.

An increase of compressibility significantly reduces the resonance frequency. This effect is enhanced at the higher relative thicknesses d_0/R_{20}, or shear moduli, and a smaller Poisson ratio. In particular, when the bubble radius decreases at fixed thickness, this effect of compressibility will become relatively more important. Compressibility thus introduces a dependence of the frequency on the shell radius that is more complex than in the incompressible case, where $\omega_0 \propto 1/R_{20}$ in the thin shell limit.

For large values of G', Eq. (46) yields, after setting $K' = [2(1+\nu)/3(1-2\nu)]G' \equiv f(\nu)G'$,

$$\omega_{0,G' \gg \hat{P}}^2 = \frac{1}{\rho_f R_{20}^2} \left(4G' \frac{R_{20}^3 - R_{10}^3}{R_{20}^3} \right) \frac{3f(\nu)}{4 + 3f(\nu)\frac{R_{10}^3}{R_{20}^3}}. \tag{55}$$

Then

$$\left(\frac{\omega_{0,G' \gg \hat{P}}}{\omega_{0,G' \gg \hat{P}}^{inc}} \right)^2 = \frac{3f(\nu)\left(1 - \frac{d_0}{R_{20}}\right)^3}{4 + 3f(\nu)\left(1 - \frac{d_0}{R_{20}}\right)^3} \equiv g(\nu, d_0, R_{20}). \tag{56}$$

In the thin shell limit, compressibility leads to a decrease in the pulsation squared by a factor $\sqrt{f(\nu)/[f(\nu) + 4/3]}$.

Equation (55) can also be interpreted from the following practical viewpoint: if one measures a shell pulsation

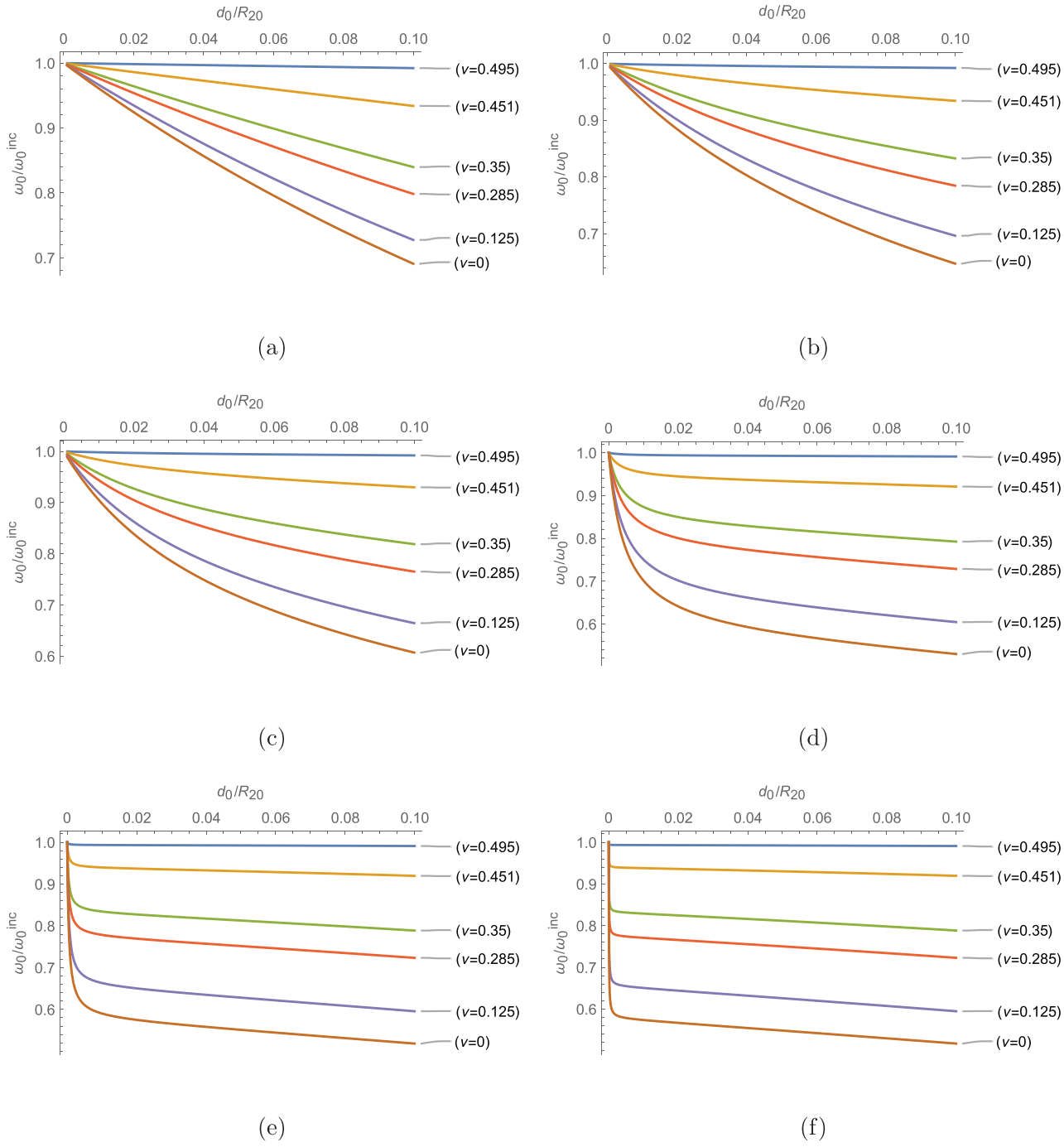

FIG. 1. (Color online) Ratio of the undamped resonance frequencies ω_0/ω_0^{inc} as a function of d_0/R_{20}, in the absence of external surface tension. G' is fixed to (a) $G' = \tilde{P}$, (b) $G' = 5\tilde{P}$, (c) $G' = 10\tilde{P}$, (d) $G' = 100\tilde{P}$, (e) $G' = 1000\tilde{P}$, (f) $G' = 10^4\tilde{P}$. $\tilde{P}$ is $P_{G_0} - 2\gamma_1/3\kappa R_{10}$. We varied K' as $100\,G'$, $10\,G', 3\,G', 2\,G'$, G', and $\frac{2}{3}\,G'$, and the corresponding Poisson ratios $\nu = (3K' - 2G')/(6K' + 2G')$ are shown on each curve. Note that when $\nu = -1$, $\omega_0 \approx 0$.

and deduces from this measurement a value G'_0 for the shell, assuming incompressibility, the same measurement can also be obtained with a shell of shear modulus G' and Poisson ratio ν obeying $G'_0 = G'g(\nu, d_0, R_{20})$.

The consequences are twofold: as $g(\nu, d_0, R_{20})$ is significantly smaller than 1, as soon as $\nu < 1/2$, the existence of unforeseen compressibility will lead to an underestimation of the shear modulus. For instance, for a shell of estimated thickness 15 nm and external radius 2 μm, if ν happens to be 0.4 instead of 0.5, $g(\nu, d_0, R_{20}) = 0.77$, which means that the shear modulus will be underestimated by 23%. This value reaches 28% if $d_0 = 200$ nm.

Second, as g is an increasing function of R_{20}, using a model for incompressible material can lead to an artificial increase in the (apparent) shear modulus with the radius, a feature regularly pointed out in the literature.

These compressibility effects are more pronounced for thick shells, and we are not aware of oscillation

https://doi.org/10.1121/10.0003500

measurements in the literature based on thick shells like polymeric shells. In addition, a more quantitative analysis of the impact of compressibility on the radius dependence of the frequency, by comparison with other suggestions like nonlinear effects, requires us to know more about the inner pressure inside the considered shells, which depends on their manufacturing process and also potentially on the allotted time for pressure equalization through transmembrane diffusion. This point becomes even more evident in the zero-thickness shell limit that is discussed in the following.

I. Discussion: From finite thickness to zero-thickness shell

For vanishing thickness, considering the corresponding limit in our finite thickness model or in that of Church (1995) leads to models that can be compared to zero-thickness models. In particular, in Hoff *et al.* (2000), the vanishing thickness limit of the Church model is considered, and the resulting frequency is shown to be similar to that obtained in de Jong *et al.* (1992) or in the linearized version of Marmottant *et al.* (2005):

$$\omega_0^{0-\text{thickness}} = (\rho_f R_0^2)^{-1/2}\left(3\kappa P_{G0} + 4\frac{\chi_0}{R_0},\right)^{1/2}, \tag{57}$$

where R_0 is the shell radius and χ_0 has the dimension of a surface tension and includes in-plane elasticity effects as well as surface tension effects on both sides of the interface (de Jong *et al.*, 1992; Hoff *et al.*, 2000; Marmottant *et al.*, 2005; Sarkar *et al.*, 2005; van der Meer *et al.*, 2007). In Hoff *et al.* (2000), when surface tension effects are neglected, χ_0 is shown to be equal to $\chi_{2D} = 3G'd_0$, the in-plane surface contraction modulus.

We examine here the small-thickness limit of our model. We consider only the incompressibility limit, which is already an interesting source for discussion and allows direct comparison with the actual zero-thickness models.

Keeping only the zeroth and first orders in d_0/R_{20} in Eq. (46), we find the following expansion:

$$\omega_0^{inc} = (\rho_f R_{20}^2)^{-1/2}\left[3\kappa P_{G0} - \frac{2\gamma_1}{R_{20}} - \frac{2\gamma_2}{R_{20}} + \left(12G' + 9\kappa P_{G0} - \frac{8\gamma_1}{R_{20}}\right)\frac{d_0}{R_{20}} + o\left(\frac{d_0}{R_{20}}\right)\right]^{1/2}. \tag{58}$$

By comparison with Eq. (57), this introduces a correction that implies that pressure and inner surface tension have a more complex spatial dependence than that proposed in the Church–Hoff model, where the first order in d_0/R_{20} was neglected in the inertial term.

We attempt to discuss the implication of our modeling regarding the interpretation of experimental data. Authors generally consider a given experiment for a set of shells of different sizes, which they either watch [measuring thus the radius oscillation (Chetty *et al.*, 2008; Doinikov *et al.*, 2009; Li *et al.*, 2013; Tu *et al.*, 2009; van der Meer *et al.*, 2007)] or listen to [measuring thus the acoustic transmission (Parrales *et al.*, 2014)]. The obtained curves are then fitted according to the chosen model, which results in the determination of the corresponding elastic modulus for each shell radius. It is then generally observed that this constant increases with the radius, which highlights the limit of the chosen model. Other parameters are generally considered as known, but they are not always given by the authors. In particular, the inner pressure P_{G0} is sometimes set to atmospheric pressure without much justification (Doinikov *et al.*, 2009; Li *et al.*, 2013; Tu *et al.*, 2009; van der Meer *et al.*, 2007), but some authors do not specify their choice (Parrales *et al.*, 2014). On the other hand, the descriptions of fabrication processes of home-made microshells often mention initial gas pressure larger than 1 bar (Parrales *et al.*, 2014; Segers *et al.*, 2016), which calls into question the hypothesis of atmospheric pressure inside the shells. Though diffusion may favor this hypothesis, such a phenomenon will also induce stresses inside the shell reaching its new equilibrium, resulting in uncertainties about the exact state around which the oscillations take place.

Finally, it is generally observed in all papers that while the radius varies by a factor of 2–3, the corresponding elastic modulus varies by a factor of 3–4. In Parrales *et al.* (2014), this is the case, but contrary to most other papers, where only the values of the elastic constants are given, the measured frequencies are also mentioned. We therefore use these raw data to make the following comments. In Fig. 2, the pulsations found in the experiments are plotted as a function of shell radius. Those shells are lipidic shells; therefore, the small-thickness limit holds. The fit of their data by the usual zero-thickness law [Eq. (57), assuming $P_{G0} = 1$ bar and $\kappa = 1.4$] is not that good, which illustrates

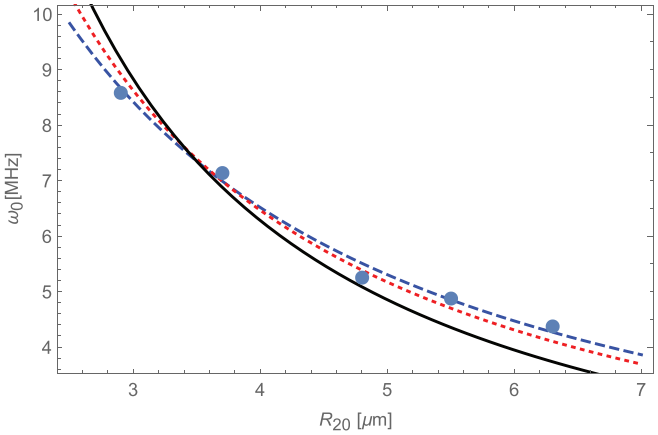

FIG. 2. (Color online) Dots: experimental pulsations found in Parrales *et al.* (2014) as a function of shell radius. Full black line: fit with Eq. (57) with fixed inner pressure $P_{G0} = 1$ bar and χ_0 as a free parameter. Red dotted line: fit with the same equation, but the pressure is also a free parameter. Blue dashed line: fit with Eq. (58) with also the surface tension being a free parameter. Using Eq. (58) allows the recovery of the full spatial dependence of the data, with a $1/R_0$ and a $1/R_0^{3/2}$ contribution.

the conclusions of the authors who, considering each radius separately, showed that the elastic modulus must be an increasing function of the radius. We note, however, that the fit yields $\chi_0 = 0.21$ N/m, which is smaller than all the values reported by the author for the different shell radii, which calls into question the (implicit) choice of inner pressure or of polytropic constant they made. Interestingly, letting P_{G0} free leads to a better fit, with $P_{G0} = 1.6$ bar. This shows the importance of the knowledge of the inner pressure or, equivalently, of the polytropic coefficient that depends on the chosen gas and on the details of the thermodynamics process, as discussed in Parrales *et al.* (2014).

In the expression for the zero-thickness limit that we established [Eq. (58)], we show that the contribution of pressure is more complex and that it is important to decouple, in the elastic contribution of the interface, bulk effects from surface tension effects: they do not sum up in a simple χ_0 parameter. Using this expression, we find an even better fit for the data of Parrales *et al.* (2014), illustrating thus the complex interplay between all the parameters of these models. Note that we do not claim here that the parameters we find are those that actually characterize the considered shell. Our discussion simply highlights the need for a good knowledge of a maximum of parameters, if one wishes to extract one unknown parameter from the sole measurement of oscillation frequencies.

J. Discussion: Effect of compressibility on the damping

Reminder: Our model assumes that $\tau_S = \mu_M/M'$ is much smaller than ω_0^{-1}. In the following examples, we checked that $\tau_S\omega_0$ is always lower than 0.01. We set here the fluid viscosity $\mu_f = 0.001$ Pa·s and the shear viscosity $\mu_G = 0.002$ Pa·s.

As for the discussion on pulsation, we set $\gamma_2 = 0$ and consider several values of $\tilde{P} = P_{G_0} - (2\gamma_1/3\kappa R_{10})$. In Fig. 3, we show the ratio of the damping constants δ/δ^{inc} under the hypothesis that μ_K varies with μ_G the same way K' varies with G', i.e., the viscous and elastic Poisson ratio are equal (Lemaitre and Chaboche, 1994). In Fig. 4, μ_K is chosen to be equal to $0.7\mu_G$ following Pritz (2009), where it is shown that $2/3 < \mu_K/\mu_G < 1$ for thermodynamic consistency.

Compressibility has the effect of making the damping constant decrease. As for the elastic constant determined through the frequency, this may lead to an underestimation

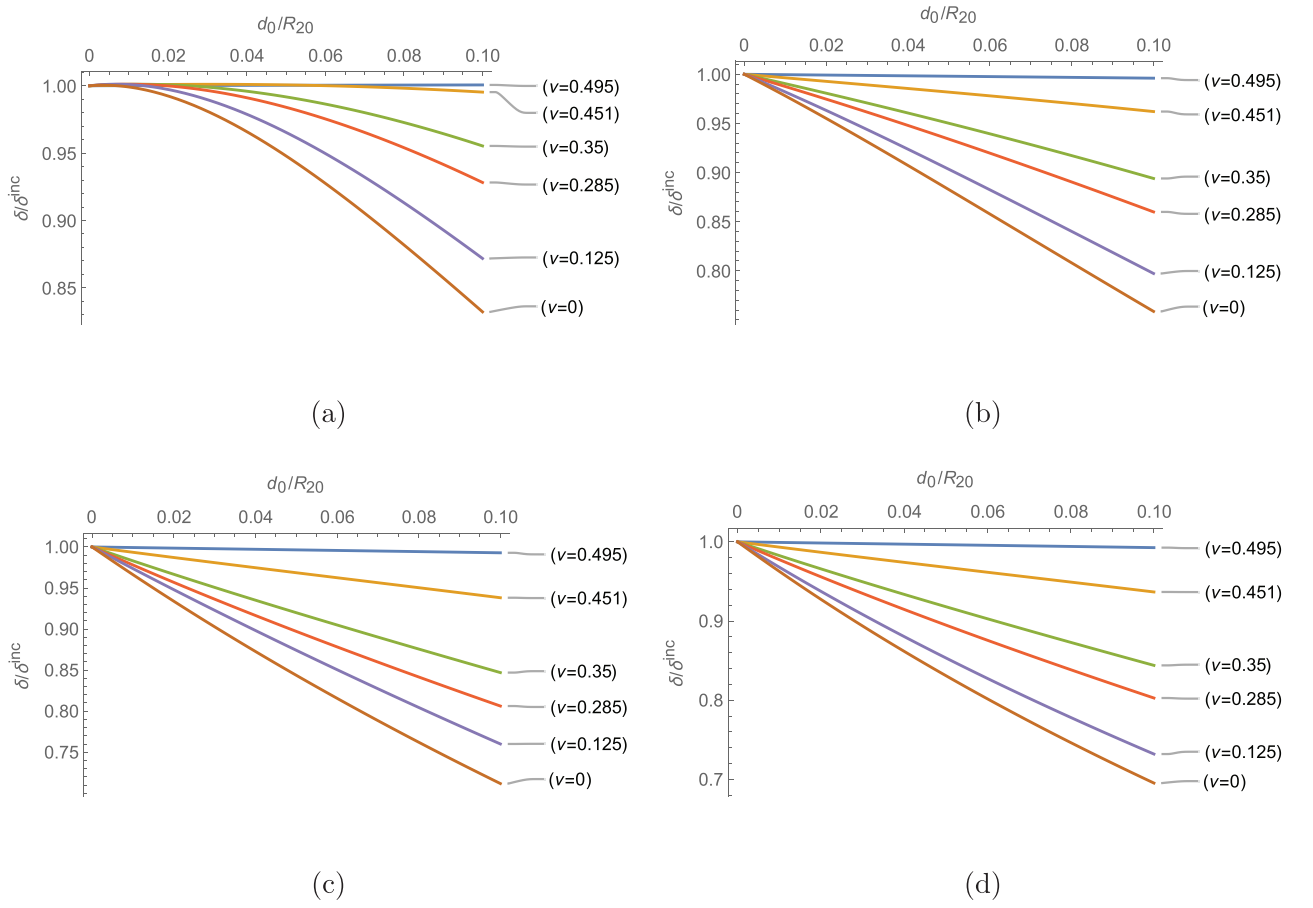

FIG. 3. (Color online) Ratio of the damping ratios δ/δ^{inc} as a function of d_0/R_{20}, in the absence of external surface tension. G' is fixed to (a) $G' = \tilde{P}$, (b) $G' = 1.5\,\tilde{P}$, (c) $G' = 4\,\tilde{P}$, (d) $G' = 5\,\tilde{P}$. $\tilde{P}$ is $P_{G_0} - (2\gamma_1/3\kappa R_{10})$. We varied K' as $100\,G'$, $10\,G'$, $3\,G'$, $2\,G'$, G', and $\frac{2}{3}\,G'$, and the corresponding Poisson ratios $\nu = (3K' - 2G')/(6K' + 2G') = (3\mu_K - 2\mu_G)/(6\mu_K + 2\mu_G)$ are shown on each curve. Note that curves do not vary by more than 1% for $G' \geq 5\,\tilde{P}$.

https://doi.org/10.1121/10.0003500

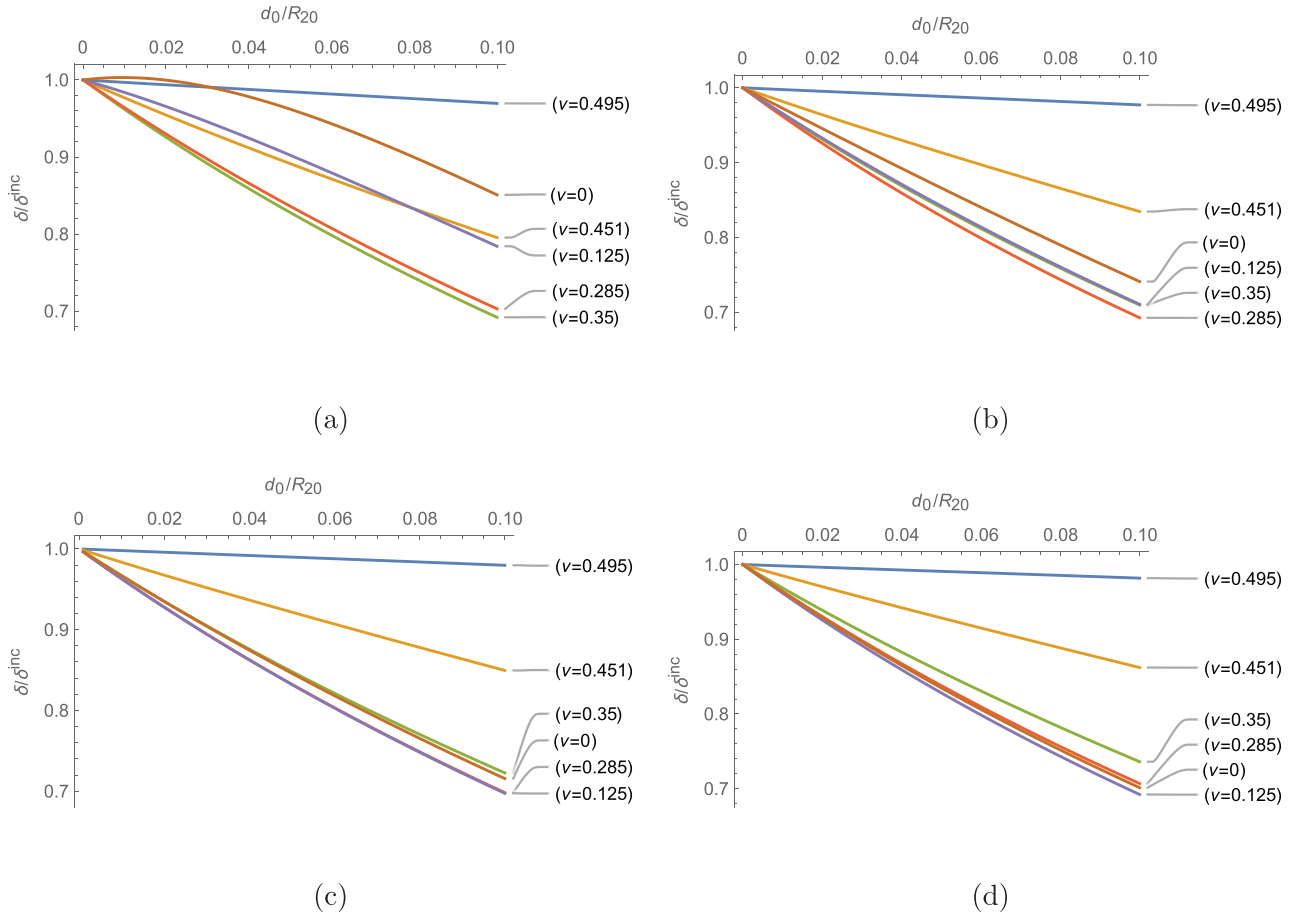

FIG. 4. (Color online) Ratio of the damping ratios δ/δ^{inc} as a function of d_0/R_{20}, in the absence of external surface tension. G' is fixed to (a) $G' = \tilde{P}$, (b) $G' = 2\tilde{P}$, (c) $G' = 3\tilde{P}$, (d) $G' = 5\tilde{P}$. $\tilde{P}$ is $P_{G_0} - (2\gamma_1/3\kappa R_{10})$. We varied K' as $100\,G', 10\,G', 3\,G', 2\,G'$, G', and $\frac{2}{3}\,G'$, and the corresponding Poisson ratios $\nu = (3K' - 2G')/(6K' + 2G')$ are shown on each curve. Note that curves do not vary by more than 1% for $G' \geq 5\,\tilde{P}$. In all cases, $\mu_K = 0.7\mu_G$, following Pritz (2009).

of the shear viscosity if an incompressible model is used. For large values of G' and $K' = G'f(\nu)$ compared to $\tilde{P}$, as for the frequencies, the damping depends only on elastic properties through the Poisson ratio, as can be seen through Eqs. (41) and (42) taken in the limit $G', K' \gg \tilde{P}$. In practice, as seen in Figs. 3 and 4, this limit is reached as soon as $G' > 5\tilde{P}$, which is generally the case for actual commercial UCAs. Interestingly, the choice of the model for the viscous Poisson ratio has little impact on the final results: for high values of K', μ_K is not expected to contribute much for both models, as its contribution vanishes in the incompressibility limit [see Eq. (53)], and for values of K' comparable to G', μ_K is close to μ_G in both models. If the Pritz (2009) model is assumed though, the coupling between elastic and viscous terms is such that the damping is not a monotonous function of the Poisson ratio ν.

VI. TRANSVERSE ISOTROPIC ELASTIC SHELL

We now examine the effect of anisotropy in the properties of a purely elastic material. We reformulate Eq. (4) using elastic constants corresponding to standard deformations (Itskov and Aksel, 2002; Lempriere, 1968):

$$\begin{cases} \sigma^{el}_{rr} = \dfrac{(1-\nu_{||})E'_r}{1-\nu_{||}-2\dfrac{E'_{||}}{E'_r}\nu^2_{\theta r}}\epsilon_{rr} + \dfrac{2\nu_{\theta r}E'_{||}}{1-\nu_{||}-2\dfrac{E'_{||}}{E'_r}\nu^2_{\theta r}}\epsilon_{\theta\theta}, \\ \sigma^{el}_{\theta\theta} = \sigma^{el}_{\phi\phi} = \dfrac{\nu_{\theta r}E'_{||}}{1-\nu_{||}-2\dfrac{E'_{||}}{E'_r}\nu^2_{\theta r}}\epsilon_{rr} + \dfrac{E'_{||}}{1-\nu_{||}-2\dfrac{E'_{||}}{E'_r}\nu^2_{\theta r}}\epsilon_{\theta\theta}, \end{cases} \tag{59}$$

where E'_r is the Young modulus for traction in the radial direction, while $E'_{||}$ is the Young modulus in the orthoradial plane. $\nu_{||}$ is the Poisson ratio in this same plane, and $\nu_{\theta r}$ is the Poisson ratio governing deformations in the orthoradial plane when there is a radial load.[1]

Thermodynamical consistency imposes (Lempriere, 1968)

$$\begin{aligned} &-1 \leq \nu_{||} \leq 1, \\ &-\sqrt{E'_r/E'_{||}} \leq \nu_{\theta r} \leq \sqrt{E'_r/E'_{||}}, \\ &\nu_{||} \leq 1 - 2\nu^2_{\theta r}\frac{E'_{||}}{E'_r}. \end{aligned} \tag{60}$$

For an isotropic material of Poisson ratio ν, these inequalities reduce to $-1 \leq \nu \leq 1/2$. The case $\nu = 1/2$

corresponds to incompressible material as considered in Church (1995).

A. Displacement within the shell

Following the same steps as in Sec. V A, the displacement now obeys the following equation:

$$\frac{d^2u}{dr^2}+\frac{2}{r}\frac{du}{dr}-\frac{2ku}{r^2}=0, \tag{61}$$

with

$$k=\frac{E'_{\parallel}(1-\nu_{\theta r})}{E'_r(1-\nu_{\parallel})}, \tag{62}$$

which is the equivalent of Eq. (9) for this purely elastic case.

The solutions of Eq. (61) have the form

$$u^{Tr}(r)=a^{Tr}r^{\beta_+}+b^{Tr}r^{\beta_-}, \tag{63}$$

with $\beta_{\pm}=\frac{1}{2}\left(-1\pm\sqrt{1+8k}\right)$. Note that by virtue of Eq. (60), it can be shown that $k\geq -1/8$ whatever the material properties and therefore the exponents $\beta_{\pm}$ are real. The isotropic case corresponds to $k=1$ then $\beta_-=-2$ and $\beta_+=1$. The variables a_T and b_T are related to the boundary conditions thanks to Eq. (7):

$$a^{Tr}=\frac{(R_2-R_{2e})R_{10}^{\beta_-}-(R_1-R_{1e})R_{20}^{\beta_-}}{R_{10}^{\beta_-}R_{20}^{\beta_+}-R_{10}^{\beta_+}R_{20}^{\beta_-}} \tag{64}$$

and

$$b^{Tr}=\frac{(R_1-R_{1e})R_{20}^{\beta_+}-(R_2-R_{2e})R_{10}^{\beta_+}}{R_{10}^{\beta_-}R_{20}^{\beta_+}-R_{10}^{\beta_+}R_{20}^{\beta_-}}. \tag{65}$$

The Rayleigh–Plesset-like equation can be derived following the same steps as in Sec. V C. For the sake of simplicity, we calculate directly the resonance frequency in Sec. VI B.

B. Resonance frequency

Following the same steps as in Sec. V E, one gets the following system:

$$M\ddot{X}+KX=F(t), \tag{66}$$

where

$$X=\begin{pmatrix}x\\y\end{pmatrix},\ F(t)=\begin{pmatrix}-P_{ac}(t)\\0\end{pmatrix},\ M=\begin{bmatrix}0&\rho_f R_{20}^2\\0&0\end{bmatrix},$$

and

$$K^{Tr}=\begin{bmatrix}k_{11}^{Tr}&\dfrac{-2\gamma_2}{R_{20}}\\k_{21}^{Tr}&k_{22}^{Tr}\end{bmatrix}, \text{where}$$

$$\begin{aligned}k_{11}^{Tr}=&\left(3\kappa P_{G_0}-\frac{2\gamma_1}{R_{10}}\right)\left\{1-2\frac{(R_{20}^{\beta_+-1}-R_{10}^{\beta_+-1})(\beta_+-1)^{-1}R_{10}^{\beta_-}A_+-(R_{20}^{\beta_--1}-R_{10}^{\beta_--1})(\beta_--1)^{-1}R_{10}^{\beta_+}A_-}{E'_r(1-\nu_{\parallel})(\beta_+-\beta_-)}\right\}\\&+\frac{2(R_{20}^{\beta_+-1}-R_{10}^{\beta_+-1})(\beta_+-1)^{-1}R_{10}^{\beta_-}A_+\left[E'_r(1-\nu_{\parallel})\beta_-+2\nu_{\theta r}E'_{\parallel}\right]}{\left(1-\nu_{\parallel}-2\dfrac{E'_{\parallel}}{E'_r}\nu_{\theta r}^2\right)E'_r(1-\nu_{\parallel})(\beta_+-\beta_-)}\\&-\frac{2(R_{20}^{\beta_--1}-R_{10}^{\beta_--1})(\beta_--1)^{-1}R_{10}^{\beta_+}A_-\left[E'_r(1-\nu_{\parallel})\beta_++2\nu_{\theta r}E'_{\parallel}\right]}{\left(1-\nu_{\parallel}-2\dfrac{E'_{\parallel}}{E'_r}\nu_{\theta r}^2\right)E'_r(1-\nu_{\parallel})(\beta_+-\beta_-)},\end{aligned} \tag{67}$$

with

$$A_+=\beta^+(1-\nu_{\parallel})E'_r-\left[1-(2-\beta^+)\nu_{\theta r}\right]E'_{\parallel}, \tag{68}$$

$$A_-=\beta^-(1-\nu_{\parallel})E'_r-\left[1-(2-\beta^-)\nu_{\theta r}\right]E'_{\parallel}, \tag{69}$$

and

$$\begin{aligned}k_{21}^{Tr}=&-3\kappa P_{G_0}+\frac{2\gamma_1}{R_{10}}\\&+\frac{R_{20}^{\beta_+}R_{10}^{\beta_-}\left[E'_r(1-\nu_{\parallel})\beta_-+2\nu_{\theta r}E'_{\parallel}\right]}{\left(1-\nu_{\parallel}-2\dfrac{E'_{\parallel}}{E'_r}\nu_{\theta r}^2\right)\left(R_{10}^{\beta_-}R_{20}^{\beta_+}-R_{10}^{\beta_+}R_{20}^{\beta_-}\right)}\\&-\frac{R_{20}^{\beta_-}R_{20}^{\beta_+}\left[E'_r(1-\nu_{\parallel})\beta_++2\nu_{\theta r}E'_{\parallel}\right]}{\left(1-\nu_{\parallel}-2\dfrac{E'_{\parallel}}{E'_r}\nu_{\theta r}^2\right)\left(R_{10}^{\beta_-}R_{20}^{\beta_-}-R_{10}^{\beta_+}R_{20}^{\beta_-}\right)},\end{aligned} \tag{70}$$

https://doi.org/10.1121/10.0003500

$$k_{22}^{Tr} = \frac{R_{20}R_{10}^{\beta_- + \beta_+ - 1}\left[E_r'(1-\nu_{||})(\beta_+ - \beta_-)\right]}{\left(1 - \nu_{||} - 2\frac{E_{||}'}{E_r'}\nu_{\theta r}^2\right)(R_{10}^{\beta_-}R_{20}^{\beta_+} - R_{10}^{\beta_+}R_{20}^{\beta_-})}. \quad (71)$$

Then the undamped resonance frequency is

$$\omega_0^{Tr} = \left(\frac{\det[K^{Tr}]}{m_{12}k_{21}^{Tr}}\right)^{1/2}. \quad (72)$$

C. Discussion: Effect of anisotropy on ω_0

In what follows, the couple $(E' = 2G'(1+\nu),\nu)$ will be used to describe the elastic properties of an isotropic solid for the sake of comparison with the elastic properties of a transversely isotropic material.

We first discuss what is the impact of anisotropy keeping the material incompressible. In such a situation, it is shown in Itskov and Aksel (2002) that $\nu_{\theta r} = 1/2$, while $\nu_{||} = 1 - (E_{||}'/2E_r')$. Thermodynamics constraints [Eq. (60)] then impose $E_r' > E_{||}'/4$.

We remark that Eq. (62). becomes $k = 1$, i.e., the deformation function is the same as in the isotropic case. Second, the terms in the K^{Tr} matrix implying the shell elastic constants are all proportional to E_r' and do not depend on $E_{||}'$. We conclude that incompressible shells oscillate exactly the same way whatever the value of their in-plane Young modulus, i.e., they oscillate like isotropic incompressible shells of Young modulus E_r'.

For anisotropic compressible material, in general, hydrostatic stress does not necessarily induce a uniform dilatation in the three directions. It is interesting for comparison with the isotropic case to consider the situation where this is true. In such a situation of isotropic volumetric response, a bulk modulus can be defined as a material constant (Itskov and Aksel, 2002). It is equal to $\varkappa = E_r'/[3(1-2\nu_{\theta r})]$. In addition, it can be shown that $\nu_{||}$ is given by $1 - E_{||}'/2(1/E_r' + 1/3\varkappa)$; the material properties are thus described, for the radial motion considered here, by three independent variables (e.g., $\varkappa$, E_r' and $E_{||}'$) instead of four in the general case and two in the incompressible case. In this case also, the pulsation is that of the isotropic material of moduli $K' = \varkappa$ and $E' = E_r'$, though the deformation inside the shell is not the same: in Eq. (62), k is independent from $E_{||}'$ (but not necessarily equal to 1), and because $\nu_{||}$ appears only under the pattern $1 - \nu_{||}$ in K^{Tr}, it can be easily seen that the contribution of $E_{||}'$ vanishes.

Finally, in Fig. 5, we consider a general (arbitrary) case, based on the test case of the configuration $\mathcal{R}$ as it refers to a lipidic shell, which we may expect to exhibit transverse anisotropic properties. We have fixed $\nu_{||} = \nu_{\theta r} = 0.35$ and varied $E_{||}'$ as a function of E_r', within the bounds allowed by thermodynamics. Here, $E_{||}'$ also influences the frequency, which increases as $E_{||}'$ increases.

In all cases, as for the isotropic case, these results show that for a given measure of pulsation frequency, several sets of elastic parameters can yield the same result. More complex dependence with the external radius is also expected.

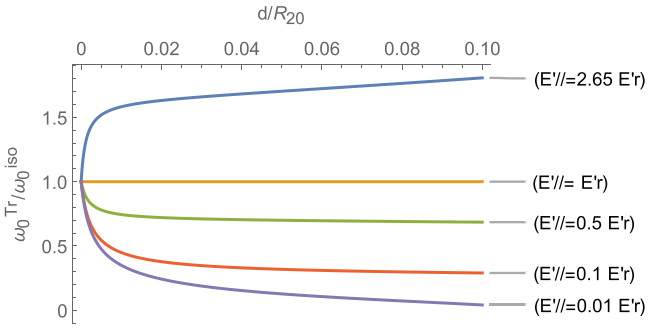

FIG. 5. (Color online) Ratio of the undamped resonance frequencies in the compressible case $\omega_0^{Tr}/\omega_0^{iso}$. The values for the in-plane and out-plane Poisson ratio are $\nu_{||} = \nu_{\theta r} = 0.35$. We varied $E_{||}'$ as $0.01\,E_r'$, $0.1\,E_r'$, $0.5\,E_r'$, E_r' and $2.65\,E_r'$; the isotropic constants $E' = E_r'$ and ν are set to 88.8 MPa and 0.35, respectively.

VII. CONCLUSION AND PERSPECTIVES

We have developed a finite thickness shell model for the oscillations of an encapsulated bubble whose material can be compressible and/or present different elastic properties in the radial and orthoradial directions. The main hypothesis is that we have neglected the mass of the shell, leading to infinite velocity for wave propagation in the material, to simplify the equations. The next step would be to consider the complete problem of wave propagation, as done for instance in Doinikov *et al.* (2018) and Doinikov and Marmottant (2018) for a bubble oscillating in a liquid confined by a viscoelastic solid.

We have found exact expressions for the free pulsation of an encapsulated bubble, which could be used to interpret more accurately experimental characterization of UCAs. Our results suggest that neglecting compressibility will lead to underestimation of the shear modulus and that adding some compressibility in the model may explain the apparent growth of the elastic moduli with the shell radius.

Due to the growing interest in the development of new generation UCAs, made of various material and built with well defined radii, we expect that several opportunities to test our model will emerge in the near future. Our predictions can also be used to build more complete theories accounting for the response of the shells to external signals.

ACKNOWLEDGMENTS

The authors appreciate fruitful discussions with Philippe Marmottant and Salvatore Federico.

APPENDIX: DEFORMATION VELOCITIES

We present here the expressions obtained for $\dot{a}$ and $\dot{b}$ by directly deriving a and b (see Sec. V B):

$$\dot{a}(t) = \frac{R_2^2 U_2 - R_1^2 U_1}{R_3^2 - R_1^3} + \frac{U_2}{(R_2^3 - R_1^3)^2} \times \left[(R_1 - R_{1e})(3R_1^2 R_2^2) - (R_2 - R_{2e})(R_2^4 + 2R_2 R_1^3)\right] + \frac{U_1}{(R_2^3 - R_1^3)^2}\left[(R_2 - R_{2e})(3R_1^2 R_2^2) - (R_1 - R_{1e})(R_1^4 + 2R_1 R_2^3)\right]$$

and

$$\dot{b}(t) = \frac{(R_2 U_1 - R_1 U_2) R_1^2 R_2^2}{R_3^2 - R_1^3} + \frac{U_1}{(R_2^3 - R_1^3)^2} \times \left[(R_1 - R_{1e})(2R_1 R_2^6 + R_1^4 R_2^3) - (R_2 - R_{2e})(3R_1^2 R_2^5)\right] + \frac{U_2}{(R_2^3 - R_1^3)^2}\left[(R_2 - R_{2e})(2R_2 R_1^6 + R_2^4 R_1^3) - (R_1 - R_{1e})(3R_1^5 R_2^2)\right].$$

[1]Note that $\nu_{r\theta}$ is used by some authors instead of $\nu_{\theta r}$ (Lempriere, 1968).

Abou-Saleh, R. H., Peyman, S. A., Critchley, K., Evans, S. D., and Thomson, N. H. (**2013**). "Nanomechanics of lipid encapsulated microbubbles with functional coatings," Langmuir **29**(12), 4096–4103.

Altenbach, H., Brigadnov, I. A., and Eremeyev, V. A. (**2008**). "Oscillations of a magneto-sensitive elastic sphere," J. Appl. Math. Mech. **88**(6), 497–506.

Besant, W. H. (**1859**). *A Treatise on Hydrostatics and Hydrodynamics* (Deighton, Bell, and Co., London).

Buchner Santos, E., Morris, J. K., Glynos, E., Sboros, V., and Koutsos, V. (**2012**). "Nanomechanical properties of phospholipid microbubbles," Langmuir **28**(13), 5753–5760.

Campbell, S., Griffin, D. R., Pearce, J. M., Diaz-Recasens, J., Cohen-Overbeek, T., Willson, K., and Teague, M. J. (**1983**). "New doppler technique for assessing uteroplacental blood flow," Lancet **321**(8326), 675–677.

Chatterjee, D., and Sarkar, K. (**2003**). "A Newtonian rheological model for the interface of microbubble contrast agents," Ultrasound Med. Biol **29**(12), 1749–1757.

Chetty, K., Stride, E., Sennoga, C. A., Hajnal, J. V., and Eckersley, R. J. (**2008**). "High-speed optical observations and simulation results of SonoVue microbubbles at low-pressure insonation," IEEE Trans. Ultrason. Ferroelectr. Freq. Control **55**(6), 1333–1342.

Church, C. C. (**1995**). "The effects of an elastic solid surface layer on the radial pulsations of gas bubbles," J. Acoust. Soc. Am. **97**(3), 1510–1521.

Coupier, G., Djellouli, A., and Quilliet, C. (**2019**). "Let's deflate that beach ball," Eur. Phys. J. E **42**(9), 129.

Dalenbring, M. (**2002**). "An explicit formulation of a three-dimensional material damping model with transverse isotropy," Int. J. Sol. Struct. **39**(1), 225–249.

de Jong, N., Cornet, R., and Lancee, C. (**1994**). "Higher harmonics of vibrating gas-filled microspheres. Part one: Simulations," Ultrasonics **32**(6), 447–453.

de Jong, N., and Hoff, L. (**1993**). "Ultrasound scattering properties of albunex microspheres," Ultrasonics **31**(3), 175–181.

de Jong, N., Hoff, L., Skotland, T., and Bom, N. (**1992**). "Absorption and scatter of encapsulated gas filled microspheres: Theoretical considerations and some measurements," Ultrasonics **30**(2), 95–103.

Doinikov, A. A., and Dayton, P. A. (**2006**). "Spatio-temporal dynamics of an encapsulated gas bubble in an ultrasound field," J. Acoust. Soc. Am. **120**(2), 661–669.

Doinikov, A. A., Dollet, B., and Marmottant, P. (**2018**). "Model for the growth and the oscillation of a cavitation bubble in a spherical liquid-filled cavity enclosed in an elastic medium," Phys. Rev. E **97**, 013108.

Doinikov, A. A., Haac, J. F., and Dayton, P. A. (**2009**). "Modeling of nonlinear viscous stress in encapsulating shells of lipid-coated contrast agent microbubbles," Ultrasonics **49**(2), 269–275.

Doinikov, A. A., and Marmottant, P. (**2018**). "Natural oscillations of a gas bubble in a liquid-filled cavity located in a viscoelastic medium," J. Sound Vib. **420**, 61–72.

Dovstam, K. (**1995**). "Augmented Hooke's law in frequency domain. A three dimensional, material damping formulation," Int. J. Solids Struct. **32**(19), 2835–2852.

Errico, C., Pierre, J., Pezet, S., Desailly, Y., Lenkei, Z., Couture, O., and Tanter, M. (**2015**). "Ultrafast ultrasound localization microscopy for deep super-resolution vascular imaging," Nature **527**, 499–502.

Faez, T., Goertz, D., and De Jong, N. (**2011**). "Characterization of Definity™ ultrasound contrast agent at frequency range of 5–15 Mhz," Ultrasound Med. Biol. **37**(2), 338–342.

Goertz, D. E., de Jong, N., and van der Steen, A. F. (**2007**). "Attenuation and size distribution measurements of Definity™ and manipulated Definity™ populations," Ultrasound Med. Biol. **33**(9), 1376–1388.

Gong, Y., Cabodi, M., and Porter, T. M. (**2014**). "Acoustic investigation of pressure-dependent resonance and shell elasticity of lipid-coated monodisperse microbubbles," Appl. Phys. Lett. **104**(7), 074103.

Gorce, J.-M., Arditi, M., and Schneider, M. (**2000**). "Influence of bubble size distribution on the echogenicity of ultrasound contrast agents: A study of SonoVue™," Invest. Radiol. **35**(11), 661–671.

Gramiak, R., and Shah, P. M. (**1968**). "Echocardiography of the aortic root," Invest. Radiol. **3**(5), 356–366.

Guillot, F. M., and Trivett, D. H. (**2011**). "Complete elastic characterization of viscoelastic materials by dynamic measurements of the complex bulk and Young's moduli as a function of temperature and hydrostatic pressure," J. Sound Vib. **330**(14), 3334–3351.

Helfield, B. (**2019**). "A review of phospholipid encapsulated ultrasound contrast agent microbubble physics," Ultrasound Med. Biol. **45**(2), 282–300.

Helfield, B., Leung, B. Y., Huo, X., and Goertz, D. (**2014**). "Scaling of the viscoelastic shell properties of phospholipid encapsulated microbubbles with ultrasound frequency," Ultrasonics **54**(6), 1419–1424.

Helfield, B. L., and Goertz, D. E. (**2013**). "Nonlinear resonance behavior and linear shell estimates for Definity and Micromarker assessed with acoustic microbubble spectroscopy," J. Acoust. Soc. Am. **133**(2), 1158–1168.

Hoff, L., Sontum, P. C., and Hovem, J. M. (**2000**). "Oscillations of polymeric microbubbles: Effect of the encapsulating shell," J. Acoust. Soc. Am. **107**(4), 2272–2280.

Hu, H., Zhou, H., Du, J., Wang, Z., An, L., Yang, H., Li, F., Wu, H., and Yang, S. (**2011**). "Biocompatiable hollow silica microspheres as novel ultrasound contrast agents for *in vivo* imaging," J. Mater. Chem. **21**, 6576–6583.

Hutchinson, J. W. (**1967**). "Imperfection sensitivity of externally pressurized spherical shells," J. Appl. Mech. **34**, 49–55.

Itskov, M., and Aksel, N. (**2002**). "Elastic constants and their admissible values for incompressible and slightly compressible anisotropic materials," Acta Mech. **157**, 81–96.

Khismatullin, D. B., and Nadim, A. (**2002**). "Radial oscillations of encapsulated microbubbles in viscoelastic liquids," Phys. Fluids **14**(10), 3534–3557.

Lakes, R. S., and Wineman, A. (**2006**). "On Poisson's ratio in linearly viscoelastic solids," J. Elast. **85**(1), 45–63.

Landau, L., and Lifschitz, E. (**1986**). *Theory of Elasticity*, 3rd ed. (Elsevier Butterworth-Heinemann, Oxford).

Landau, L., and Lifschitz, E. (**1987**). *Fluid Mechanics*, 2nd ed. (Elsevier Butterworth-Heinemann, Oxford).

Langtangen, H. P., and Pedersen, G. K. (**2016**). *Scaling of Differential Equations* (Springer International Publishing, Berlin).

Lemaitre, J., and Chaboche, J.-L. (**1994**). *Mechanics of Solid Materials* (Cambridge University Press, London).

Lempriere, B. M. (**1968**). "Poisson's ratio in orthotropic materials," AIAA J. **6**(11), 2226–2227.

Li, Q., Matula, T. J., Tu, J., Guo, X., and Zhang, D. (**2013**). "Modeling complicated rheological behaviors in encapsulating shells of lipid-coated microbubbles accounting for nonlinear changes of both shell viscosity and elasticity," Phys. Med. Biol. **58**(4), 985–998.

Linn, J., Lang, H., and Tuganov, A. (**2013**). "Geometrically exact Cosserat rods with Kelvin–Voigt type viscous damping," Mech. Sci. **4**, 79–96.
Liu, B., Zhou, X., Yang, F., Shen, H., Wang, S., Zhang, B., Zhi, G., and Wu, D. (**2014**). "Fabrication of uniform sized polylactone microcapsules by premix membrane emulsification for ultrasound imaging," Polym. Chem. **5**, 1693–1701.
Lubarda, V., and Chen, M. C. (**2008**). "On the elastic moduli and compliances of transversely isotropic and orthotropic materials," J. Mech. Mat. Struct. **3**, 153–171.
Lubarda, V. A., and Asaro, R. J. (**2014**). "Viscoelastic response of anisotropic biological membranes. part II: Constitutive models," Theor. Appl. Mech. **41**, 213–231.
Lum, J. S., Dove, J. D., Murray, T. W., and Borden, M. A. (**2016**). "Single microbubble measurements of lipid monolayer viscoelastic properties for small-amplitude oscillations," Langmuir **32**(37), 9410–9417.
Lytra, A., Sboros, V., Giannakopoulos, A., and Pelekasis, N. (**2020**). "Modeling atomic force microscopy and shell mechanical properties estimation of coated microbubbles," Soft Matter **16**(19), 4661–4681.
Marmottant, P., van der Meer, S., Emmer, M., Versluis, M., de Jong, N., Hilgenfeldt, S., and Lohse, D. (**2005**). "A model for large amplitude oscillations of coated bubbles accounting for buckling and rupture," J. Acoust. Soc. Am. **118**, 3499–3505.
Mohanty, K., Papadopoulou, V., Newsome, I. G., Shelton, S., Dayton, P. A., and Muller, M. (**2019**). "Ultrasound multiple scattering with microbubbles can differentiate between tumor and healthy tissue *in vivo*," Phys. Med. Biol. **64**, 115022.
Morgan, K. E., Allen, J. S., Dayton, P. A., Chomas, J. E., Klibaov, A., and Ferrara, K. W. (**2000**). "Experimental and theoretical evaluation of microbubble behavior: Effect of transmitted phase and bubble size," IEEE Trans. Ultrason. Ferroelectr. Freq. Control **47**(6), 1494–1509.
Munglani, G., Wittel, F. K., Vetter, R., Bianchi, F., and Herrmann, H. J. (**2019**). "Collapse of orthotropic spherical shells," Phys. Rev. Lett. **123**, 058002.
Parrales, M. A., Fernandez, J. M., Perez-Saborid, M., Kopechek, J. A., and Porter, T. M. (**2014**). "Acoustic characterization of monodisperse lipid-coated microbubbles: Relationship between size and shell viscoelastic properties," J. Acoust. Soc. Am. **136**(3), 1077–1084.
Paul, S., Katiyar, A., Sarkar, K., Chatterjee, D., Shi, W. T., and Forsberg, F. (**2010**). "Material characterization of the encapsulation of an ultrasound contrast microbubble and its subharmonic response: Strain-softening interfacial elasticity model," J. Acoust. Soc. Am. **127**(6), 3846–3857.
Paul, S., Russakow, D., Rodgers, T., Sarkar, K., Cochran, M., and Wheatley, M. A. (**2013**). "Determination of the interfacial rheological properties of a poly(DL-lactic acid)-encapsulated contrast agent using *in vitro* attenuation and scattering," Ultrasound Med. Biol. **39**(7), 1277–1291.
Pitois, O., Buisson, M., and Chateau, X. (**2015**). "On the collapse pressure of armored bubbles and drops," Eur. Phys. J. E **38**(5), 48.
Plesset, M. S., and Prosperetti, A. (**1977**). "Bubble dynamics and cavitation," Annu. Rev. Fluid Mech. **9**(1), 145–185.
Pritz, T. (**2009**). "Relation of bulk to shear loss factor of solid viscoelastic materials," J. Sound Vib. **324**(3–5), 514–519.
Prosperetti, A. (**1987**). "The equation of bubble dynamics in a compressible liquid," Phys. Fluids **30**(11), 3626–3628.
Quemeneur, F., Quilliet, C., Faivre, M., Viallat, A., and Pépin-Donat, B. (**2012**). "Gel phase vesicles buckle into specific shapes," Phys. Rev. Lett. **108**, 108303.
Quilliet, C. (**2012**). "Numerical deflation of beach balls with various Poisson's ratios: From sphere to bowl's shape," Eur. Phys. J. E **35**, 48.
Rayleigh, L. (**1917**). "VIII. On the pressure developed in a liquid during the collapse of a spherical cavity," London, Edinburgh, Dublin Philos. Mag. J. Sci. **34**(200), 94–98.
Sarkar, K., Shi, W. T., Chatterjee, D., and Forsberg, F. (**2005**). "Characterization of ultrasound contrast microbubbles using in vitro experiments and viscous and viscoelastic interface models for encapsulation," J. Acoust. Soc. Am. **118**(1), 539–550.
Segers, T., de Rond, L., de Jong, N., Borden, M., and Versluis, M. (**2016**). "Stability of monodisperse phospholipid-coated microbubbles formed by flow-focusing at high production rates," Langmuir **32**(16), 3937–3944.
Segers, T., Gaud, E., Casqueiro, G., Lassus, A., Versluis, M., and Frinking, P. (**2020**). "Foam-free monodisperse lipid-coated ultrasound contrast agent synthesis by flow-focusing through multi-gas-component microbubble stabilization," Appl. Phys. Lett. **116**(17), 173701.
Shafi, A. S., McClements, J., Albaijan, I., Abou-Saleh, R. H., Moran, C., and Koutsos, V. (**2019**). "Probing phospholipid microbubbles by atomic force microscopy to quantify bubble mechanics and nanostructural shell properties," Colloids Surf. B **181**, 506–515.
Song, R., Peng, C., Xu, X., Wang, J., Yu, M., Hou, Y., Zou, R., and Yao, S. (**2018**). "Controllable formation of monodisperse polymer microbubbles as ultrasound contrast agents," ACS Appl. Mat. Int. **10**(17), 14312–14320.
Thompson, W., and Kelvin, L. (**1865**). "On the elasticity and viscosity of metals," Proc. R. Soc. Lond. A **14**, 289–297.
Tschoegl, N., Knauss, W. G., and Emri, I. (**2002**). "Poisson's ratio in linear viscoelasticity—A critical review," Mech. Time Dep. Mat. **6**, 3–51.
Tsiglifis, K., and Pelekasis, N. A. (**2008**). "Nonlinear radial oscillations of encapsulated microbubbles subject to ultrasound: The effect of membrane constitutive law," J. Acoust. Soc. Am. **123**(6), 4059–4070.
Tu, J., Guan, J., Qiu, Y., and Matula, T. J. (**2009**). "Estimating the shell parameters of SonoVue® microbubbles using light scattering," J. Acoust. Soc. Am. **126**(6), 2954–2962.
Tu, J., Swalwell, J. E., Giraud, D., Cui, W., Chen, W., and Matula, T. J. (**2011**). "Microbubble sizing and shell characterization using flow cytometry," IEEE Trans. Ultrason. Ferroelectr. Freq. Cont. **58**(5), 955–963.
van der Meer, S. M., Dollet, B., Voormolen, M. M., Chin, C. T., Bouakaz, A., de Jong, N., Versluis, M., and Lohse, D. (**2007**). "Microbubble spectroscopy of ultrasound contrast agents," J. Acoust. Soc. Am. **121**(1), 648–656.
van Rooij, T., Luan, Y., Renaud, G., van der Steen, A. F., Versluis, M., de Jong, N., and Kooiman, K. (**2015**). "Non-linear response and viscoelastic properties of lipid-coated microbubbles: DSPC versus DPPC," Ultrasound Med. Biol. **41**(5), 1432–1445.
Versluis, M., Stride, E., Lajoinie, G., Dollet, B., and Segers, T. (**2020**). "Ultrasound contrast agent modeling: A review," Ultrasound Med. Biol. **46**(9), 12117–12144.
Vilov, S., Arnal, B., and Bossy, E. (**2017**). "Overcoming the acoustic diffraction limit in photoacoustic imaging by the localization of flowing absorbers," Opt. Lett. **42**, 4379–4382.
Vincent, O., and Marmottant, P. (**2017**). "On the statics and dynamics of fully confined bubbles," J. Fluid Mech. **827**, 194–224.
Voigt, W. (**1892**). "Ueber innere reibung fester körper, insbesondere der metalle," Ann. Phys. (Berlin) **283**(12), 671–693.
von Ende, S., Lion, A., and Lammering, R. (**2011**). "On the thermodynamically consistent fractional wave equation for viscoelastic solids," Acta Mech. **221**, 1–10.
Wang, Q. X. (**2017**). "Oscillation of a bubble in a liquid confined in an elastic solid," Phys. Fluids **29**, 072101.
Wang, Q., Xue, C., Qin, Y., Zhang, X., and Li, Y. (**2020**). "The fabrication of protein microbubbles with diverse gas core and the novel exploration on the role of interface introduction in protein crystallization," Colloids Surf. A **589**, 124471.